EX LIBRIS
UNIVERSITATIS
ALBERTENSIS

The Bruce Peel
Special Collections
Library

Digitized by the Internet Archive
in 2025 with funding from
University of Alberta Library

https://archive.org/details/0162018299766

University of Alberta

Library Release Form

Name of Author: Hao Fu

Title of Thesis: Capillary Electrophoresis and Fluorescence Polarization Studies of Aptamer-protein Interactions

Degree: Master of Science

Year of This Degree Granted: 2003

Permission is hereby granted to the University of Alberta library to reproduce single copies of this thesis and to lend or sell such copies for private, scholarly, or scientific research purposes only.

The author reserves all other publication and other rights in association with the copyright in the thesis, and except as hereinbefore provided, neither the thesis nor any substantial portion thereof may be printed or otherwise reproduced in any material form whatsoever without the author's prior written permission.

University of Alberta

Capillary Electrophoresis and Fluorescence Polarization Studies of Aptamer-protein Interactions

by

HAO FU

A thesis submitted to the Faculty of Graduate Studies and Research in partial fulfillment of the requirements for the degree of

Master of Science

Department of Chemistry

Edmonton, Alberta

Fall, 2003

University of Alberta

Faculty of Graduate Studies and Research

The undersigned certify that they have read, and recommend to the Faculty of Graduate Studies and Research for acceptance, a thesis entitled **Capillary Electrophoresis and Fluorescence Polarization Studies of Aptamer-protein Interactions** submitted by **Hao Fu** in partial fulfillment of the requirements for the degree of **Master of Science**.

ABSTRACT

Affinity capillary electrophoresis (ACE) coupled with laser induced fluorescence polarization (LIFP) techniques was developed to study biomolecular interactions. The binding stoichiometries of HIV-1 reverse transcriptase (HIV-1 RT) and fluorescently-labeled single-stranded DNA aptamers RT12, RT26, RT1t49, and ODN93 were studied as an example. HIV-1 RT plays a crucial role in the life circle of HIV-1 virus, and is a marker for the virus. Aptamers that were initially developed to inhibit the activities of HIV-1 RT, were fluorescently labeled at the 5'- end and were used as detection probes. Changes in fluorescence polarization (FP) and electrophoretic mobility upon complex formation were monitored to study the binding affinity and stoichiometries. CE separated the complexes representing the 1:1 and 1:2 stoichiometries between the protein and the fluorescently-labeled aptamers. The FP of the 1:2 complex was lower compared to that of the 1:1 complex. The depolarization of the 1:2 stoichiometry was probably caused by homo-fluorescence resonance energy transfer (FRET), suggesting that the two binding sites in the HIV-1 RT were close enough to enable FRET (typically < 10 nm). An ACE/LIFP method based on the binding of fluorescent aptamers with HIV-1 RT could be useful for the analysis of the HIV-1 RT protein.

ACKNOWLEDGEMENT

I would like to thank my research director, Dr. X. Chris Le, for his guidance, support, and patience throughout this work. I would like to thank Drs. Victor Pavski, Hailin Wang, Mike Lam and James Xing; I have learned a lot from them. I would also like to thank Ms. Katerina Carastathis for her help with editing this thesis. Financial support from the Department of Chemistry at the University of Alberta and the Natural Sciences and Engineering Research Council of Canada (NSERC) is also gratefully acknowledged.

TABLE OF CONTENTS

CHAPTER 1

1 Introduction 1

1.1 Affinity capillary electrophoresis (CE) coupled with laser induced fluorescence (LIF) 1

1.2 Fluorescence polarization (FP) 3

1.3 Fluorescence energy resonance transfer (FRET) 7

1.4 Aptamers 12

1.5 HIV-1 reverse transcriptase (HIV-1 RT).....18

1.6 Thesis outline 23

1.7 References.....24

2 CE/LIF Study of Aptamers Binding with HIV-1 RT 35

2.1 Introduction 35

2.1.1 HIV-1 reverse transcriptase and aptamers.....35

2.1.2 Affinity capillary electrophoresis and laser-induced fluorescence 36

2.2 Experimental.....37

2.2.2 Reagents.....37

2.2.2 Stock solutions 38

2.2.3 Instrument 38

2.3 Results and discussion 41

2.3.1 Interaction of HIV-1 RT protein with aptamers RT12 and RT26.....42

2.3.1.1 Binding of aptamers with varying concentrations of HIV-1 RT 42

2.3.1.2 Binding of HIV-1 RT protein with varying concentrations of aptamer RT12 46

2.3.2 Interaction of HIV-1 RT protein with aptamer RT1t49.....49

2.3.3 Interaction of HIV-1 RT protein with aptamer ODN93..... 52

2.4 Conclusion.....54

2.5 References 55

3 Fluorescence polarization study of aptamers binding with HIV-1 RT.....57

3.1 Introduction 57

3.1.1 Fluorescence polarization combined with CE/LIF.....57

3.1.2 Fluorescent labeling 58

3.2 Experimental.....61

3.2.1 CE-LIFP analysis 61

3.2.2 Reagents and stock solutions 62

3.3 Results and discussion 62

3.3.1 Fluorescence polarization of complexes between aptamer

RT12 and HIV-1 RT 62

3.3.2 Fluorescence polarization of complex between aptamer RT1t49 and HIV-1 RT.....71

3.3.3 Fluorescence polarization of complex between aptamers RT26, ODN93 and HIV-1 RT 73

3.3.4 Difference in FP values and possible FRET 77

3.3.5 Effect of the stability of complexes on FP 80

3.3.6 Determination of FP value by Stop-flow 83

3.4 Conclusion.....86

3.5 References 87

4 Denaturation and storage effect on complex formation 89

4.1 Introduction 89

4.1.1 Denature of protein 89

4.1.2 Denature of DNA 90

4.1.3 Storage of samples ... .90

4.2 Experimental 91

4.3 Results and discussion 92

4.3.1 Effect of denaturation.....92

4.3.2 Effect of sample storage.....95

4.3.3 Aggregation of protein on X:1 stoichiometry 97

4.4 Conclusion 99

4.5 References 100

5 Measurement of HIV-1 RT by using RT12 as a probe 101

5.1 Introduction 101

5.2 Experimental 101

5.3 Results and discussion 102

5.4 References 107

6 Conclusion and future work.....108

LIST OF TABLES

Chapter 3

Table 3.1 MW of aptamers and HIV-1 RT 62

Table 3.2 Average FP of complexes and unbound aptamers.....77

LIST OF FIGURES

CHAPTER 1

Figure 1.1 Schematic of FP between small and large complexes 5

Figure 1.2 Fluorescence resonance energy transfer 9

Figure 1.3 Overlap integral of spectra of donor and acceptor 9

Figure 1.4 SELEX process 14

Figure 1.5 Proposed secondary structure of RT26, RT12 and RT1t49.....17

Figure 1.6 HIV-1 RT structure 20

Figure 1.8 HIV-1 RT binding with ds-DNA 22

CHAPTER 2

Figure 2.1 A schematic diagram of the CE/LIFP instrument 40

Figure 2.2 Titration of a fixed RT12 (32nM) by varying the concentration of HIV-1 RT 45

Figure 2.3 Titration of a fixed HIV-1 RT (50nM) by varying the concentration of RT12 48

Figure 2.4 Titration of a fixed RT1t49 (32nM) by varying the concentration of HIV-1 RT 50

Figure 2.5 Titration of a fixed HIV-1 RT (50nM) by varying the concentration of RT1t49 51

Figure 2.6 Titration of a fixed ODN93 (32nM) by varying the

concentration of HIV-1 RT 53

CHAPTER 3

Figure 3.1 Structure of 5-Carboxyfluorescein (5-FAM) 59

Figure 3.2 Structure of 5-FAM, after attachment to an oligonucleotide 59

Figure 3.3 Absorption and fluorescence emission spectra of 5-FAM 60

Figure 3.4 Electropherograms showing FP values of RT12 64

Figure 3.5 Electropherograms showing FP values of two complexes and RT12 65

Figure 3.6 Electropherograms showing FP values of the 1:1 complex 67

Figure 3.7 Electropherogram showing FP values of two complexes and the unbound RT12 68

Figure 3.8 Fluorescence polarization curve of two complexes and the unbound RT12 70

Figure 3.9 Electropherograms showing FP values of the 1:1 complex and the unbound aptamer RT1t49.....72

Figure 3.10 Electropherograms showing FP values of the two complexes and the unbound aptamer RT26.....75

Figure 3.11 Fluorescence polarization curve of the complexes and the unbound aptamer ODN93 76

Figure 3.12 FP as function of the HIV-1 RT concentration of the 1:2 complex containing RT12 (64 nM).....82

Figure 3.13 FP as function of the HIV-1 RT concentration of

the 1:1 complex containing RT12 (64 nM).....82

Figure 3.14 Electropherograms showing FP values of the 1:1 complex (RT1t49, non-stop flow).....84

Figure 3.15 Electropherograms showing FP values of the 1:1 complex (RT1t49, stop flow) 85

CHAPTER 4

Figure 4.1 Electropherograms showing the denaturation effect on the sample 94

Figure 4.2 Electropherograms showing the storage effect on the same sample.....96

Figure 4.3 Electropherogram showing FP values of complex of 1:1 stoichiometry and X:1 stoichiometry 98

CHAPTER 5

Figure 5.1 Calibration curve constructed using the samples containing 32 nM RT12 104

Figure 5.2 Expanded region of calibration curve constructed using the samples containing 32 nM RT12.....105

Figure 5.3 Linear region of the peak areas of the two complexes with HIV-1 RT at 0-35 nM 106

Figure 5.4 Linear region of the peak areas of RT12 with HIV-1 RT at 0-35 nM 106

Abbreviations

3TC	2', 3'-dideoxy 3'-thiacytidine
ACE	affinity capillary electrophoresis
AGE	affinity gel electrophoresis
AIDS	acquired immune deficiency syndrome
AZT	3'-azido-2', 3'-dideoxythymidine
BODIPY	4,4-difluoro-4-bora-3a, 4a-diaza-s-indancene (a trademark of Molecular Probes, Inc.)
CE	capillary electrophoresis
CZE	capillary zone electrophoresis
d4t	3'-deoxy-2',3'-didehydrothymidine
ddC	2',3'-dideoxycytidine
ddI	2',3'-dideoxyinosine
ds	double-stranded
DDW	deionized distilled water
EOF	electroosmotic flow
EMSA	electrophoretic mobility shift assay
FAM	carboxyfluorescein
FL	fluorescence
FP	fluorescence polarization
FRET	fluorescence resonance energy transfer
HIV	human immunodeficiency virus
HPLC	high performance liquid chromatography
HTS	high throughput screening
i.d.	inner diameter
LIF	laser-induced fluorescence
LIFP	laser-induced fluorescence polarization
MW	molecular weight
NNRTI	non-nucleoside reverse transcriptase inhibitor
NMR	nuclear magnetic resonance
NRTI	nucleoside reverse transcriptase inhibitor

o.d.	outer diameter
PMT	photo multiplier tube
RNase H	ribonuclease H
RT	reverse transcriptase
SELEX	systematic evolution of ligands by exponential enrichment
ss	single-stranded
TBE	Tris-borate-EDTA
Tris	Tris(hydroxymethyl) aminomethane

Chapter 1 Introduction

1.1 Affinity Capillary Electrophoresis (CE) Coupled with Laser Induced Fluorescence (LIF)

Capillary electrophoresis (CE) is a powerful technique in which an electrophoretic separation takes place in a narrow-bore capillary (typically 20-100 μm i.d., 20-100 cm long) [1-6]. CE relies on the differential migration of sample components, ideally based on their size-to-charge ratio, when an electric field is applied across a buffer-filled capillary. A high-voltage power supply (up to 30 kV) connects two buffer reservoirs via a buffer-filled capillary. Capillary efficiency is very high; the reported value ranges from 250,000 to 1 million theoretical plates, which is much higher than that of HPLC. The separation speed is very fast, ranging from milliseconds to minutes. Also, the small diameter of the capillary allows for only a very small volume of sample to be consumed, typically 3-50 nL under normal conditions.

In capillary zone electrophoresis, separation is based on the apparent mobility of an ion, μ_{app}, which is a function of the ion's effective mobility, μ_e, and electroosmotic flow, μ_{EOF}, illustrated in the following equation:

$$\mu_{app} = \mu_e + \mu_{EOF} \qquad (1\text{-}1)$$

where μ_e is a function of the charge-to-size ratio of the ion; μ_{EOF} is described by the Smoluchowski equation:

$$\mu_{EOF} = - \varepsilon \zeta / \eta \qquad (1\text{-}2)$$

where ε and η are the dielectric constant and the viscosity of the solution, respectively, and ζ is the zeta potential. Zeta potential is the electric field between the electric double layer that is formed from the surface of fused-silica silanols group to the diffuse layer, and is determined by dissociation of the silanol groups at the fused capillary wall, the charge density in the double layer, and the thickness of the diffuse layer [7-8]. Each of these parameters depends on several variables, such as pH, specific adsorption of ions in the double-layer, and ionic strength of the electrolyte solution. The dielectric constant, viscosity, and the nature of the solvent also affect on the zeta potentials [8-9]. The pH of the solution has a major effect on the zeta potential by changing the thickness of the double layer [10]. An increase in the solution pH directly influences the charge density of the capillary wall due to the increasing deprotonation of the surface silanol groups [9,11]. Under an electric field, the thickness of the diffuse layer, to which the zeta potential is directly proportional, is indirectly proportional to the square root of the ionic strength of the electrolyte solution [9,12]. Thus, the EOF decreases with increasing ionic strength of the electrolyte solution.

In general, for most CE separations, μ_{EOF} drives all the components, including anions, cations and neutral molecules from the injection to the detection end of the capillary.

CE can be used with many kinds of detection techniques, such as UV/Vis spectrometry, fluorescence, conductivity, and mass spectrometry. CE coupled with

laser-induced fluorescence (LIF) technique provides very high sensitivity. The detection limit usually ranges from 10^{-7} to 10^{-9} M, and can be narrowed down to a single molecule [13].

CE combined with molecular recognition is suitable for bioanalytical applications involving a wide variety of biomolecules, including proteins, DNA, and carbohydrates, and systems, such as antigen-antibody and enzyme-substrate [14-26]. DNA-protein interactions play a central role in a number of basic cellular processes, including DNA replication, repair, recombination, and transcription [24]. Affinity capillary electrophoresis (ACE) combines the benefits of molecular recognition with the advantages of CE (high separation efficiency and low sample consumption). LIF detection provides the additional benefit of high sensitivity. Because of the separation capability of ACE, information on binding stoichiometry can also be obtained.

1.2 Fluorescence Polarization (FP)

Perrin first described fluorescence polarization (FP), an important property of fluorescence [27-28], in 1926 [29]. Weber expanded the theory and developed the first instrumentation for the measurement of FP in the 1950s [30]. FP measurements provide information on molecular orientation and mobility, and on the processes that modulate them, including receptor-ligand interactions [31], protein-DNA interactions [32], peptide-protein binding [33], and membrane fluidity [34]. One of the most widely used FP applications is the competitive immunoassay; its first application was described for an antigen-antibody interaction in 1961 by Dandliker and Feigen [35]. When small molecules are fluorescently labeled and excited with the plane-polarized

light, the light emitted is depolarized because the fluorophore is not constrained by the rotation of the small molecule. When large complexes are formed between the target molecule and the fluorescently-labeled tracer, they rotate and tumble slowly. Therefore, the light emitted by the complex will be more polarized and the degree of polarization is higher. FP monitors the change in the size of fluorescently-labeled molecules and gives a direct measurement of the tracer bound to proteins, nucleic acids, and other biopolymers without affecting the samples [27-29, 36-37].

The FP of a molecule depends on the lifetime of fluorescence and as on the rotational relaxation time of the molecule. The rotational relaxation time ρ is the time required to rotate through the angle whose cosine is 1/*e*, or approximately 68.5°. It is described by the Stoke equation:

$$\rho = 3\,\eta V / R\,T \qquad (1\text{-}3)$$

where η is the solvent viscosity, V is the molecular volume of the fluorescent molecule, T is the temperature in degrees Kelvin, and R is the gas constant. Thus, when the viscosity and temperature are held constant, polarization is directly related to the molecular volume. Changing the size of the molecule will result in a change in polarization. The interpretation of the dependence of FP on molecular mobility is usually based on a model [38]:

$$(1/P - 1/3) = (1/P_0 - 1/3)\,(1 + 3\tau/\rho) \qquad (1\text{-}4)$$

where P_0 is the intrinsic polarization of the dye (P_0 is close to the theoretical maximum of 0.5), τ is the excited state lifetime of the dye, and ρ is the rotational relaxation time. From the equation, three conclusions can be drawn, as follows:

- FP increases as the molecular volume increases;
- FP increases as the solvent viscosity increases;
- FP decreases as the excited-state lifetime of the fluorescence increases;
- FP decreases as the temperature increases.

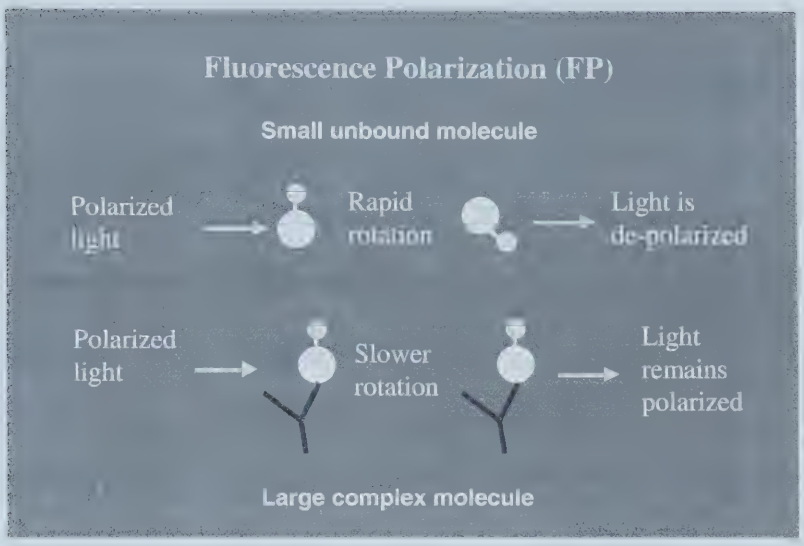

Figure 1.1 Schematic of FP in small and large complexes

As shown in Figure 1.1, small fluorescently-labeled molecules rotate quickly in the excited state and upon emission have a low polarization value. Large molecules, in this case created by the binding of a second small molecule to the first, rotate much slower during the excited state, and therefore have a high polarization value.

FP can be measured from the intensity of fluorescence at the two polarization planes, defined by the following equation [27-28]:

$$P = (I_V - I_H) / (I_V + I_H) \qquad (1\text{-}5)$$

where P is the fluorescence polarization, I_V is the intensity of the vertically-polarized fluorescence, and I_H is the intensity of the horizontally-polarized fluorescence, when vertical plane-polarized light is used for excitation. P is a dimensionless entity that can be obtained by measuring the fluorescence intensity of the two planes and does not depend on the intensity of the emitted light. Because FP is generally related to the size and shape of molecules, it can be used to monitor the binding of small fluorescent molecules to macromolecules, to study conformational changes in proteins, and to study the self-association of peptides and proteins. The theoretical limits of polarization are +1 to –1, depending on the direction of the emission. Fluorescence is usually seen to be only partially polarized or completely unpolarized.

Another measure of the polarization of fluorescence is the emission anisotropy (A), which is defined as [27-28]:

$$A = (I_V - I_H) / (I_V + 2I_H) \qquad (1\text{-}6)$$

The physical interpretation of anisotropy is similar to that of the degree of polarization, but anisotropy is used less in the literature. Analogous to polarization, the theoretical limits of anisotropy are +1 to –0.5. They can always transfer between each other from their definition:

$$A = 2P / (3-P) \qquad (1\text{-}7)$$

Although anisotropy values are preferred because they are easier to deconvolute than polarization values, the term "Fluorescence Polarization" (FP) is generally used.

FP is highly dependent on the viscosity of the solution, on the size and shape of the macromolecule (overall rotational diffusion of the macromolecule), and on the local mobility of the fluorophore. Solution viscosity is not a factor in this comparative study, because the buffer system was kept constant in all anisotropy titration experiments.

1.3 FRET (Fluorescence Energy Resonance Transfer)

Fluorescence resonance energy transfer (FRET) is a distance-dependent interaction between the electronic excited states of two or more chromophores in which excitation is transferred from a donor molecule to an acceptor molecule without emission of a photon, typically over a distance of 1-10 nm [27-28,30]. It is also called Förster energy transfer. Typically, a FRET experiment involves labeling a molecule of interest with two fluorophores, a donor and an acceptor, although a multi-donor could also be applied [39]. An important property of this transfer is that there is no emission of light by the donor; it is based on the interaction between the dipoles of a suitable donor and acceptor. A decrease in the intensity of the donor fluorescence and an increase in that of the receptor fluorescence will be observed during the process. There are three key factors that influence FRET:

- the degree of spectral overlap of the donor and acceptor molecules;
- the distance between the donor and receptor dipoles molecules, which must be in close proximity (typically 1–10 nm);
- the orientation of the two molecules, which must be approximately parallel.

FRET is a probabilistic event based on the interaction between the dipoles of a suitable donor and acceptor. Figure 1.2 shows a Jablonski schematic explanation of FRET. The donor probe is a fluorescent molecule. When light excites the fluorophore at an appropriate wavelength (250-500 nm), its electrons jump from the ground state (S_0) to a higher vibrational level (S_1, S_2, S_3, etc). Within picoseconds, these electrons decay to the lowest of these vibrational levels (S_1) and then decay more slowly (in nanoseconds) to one of the S_0 states. A photon of light is emitted whose wavelength is longer than the exciting wavelength. When a donor fluorophore is excited by incident light, and there is an acceptor in close proximity, the excited state energy from the donor can be transferred. There must be an overlap in the spectra of the donor and the acceptor, as shown in Figure 1.3. Another important factor is that the emission of the donor has a relatively high quantum yield. Molecular beacons can be considered as one type of FRET; the energy is quenched when transferred to the acceptor instead of being emitted at its own wavelength.

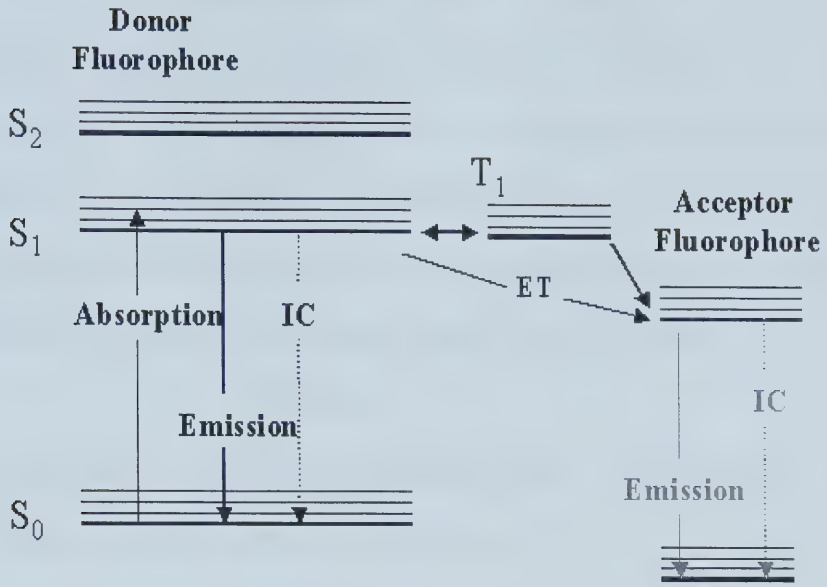

Figure 1.2 Fluorescence Resonance Energy Transfer. IC is the radiationless internal conversion to the ground state and ET is the energy transfer to a nearby fluorophore.

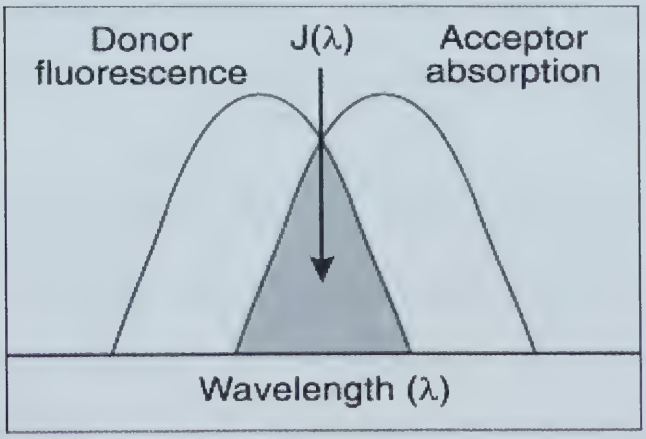

Figure 1.3 Overlap integral of spectral of donor and acceptor. J(λ) is the overlap of the donor spectrum with the absorption spectrum of the acceptor.

The singlet-singlet resonance energy transfer rate k(R) is given by:

$$k(R) = k_0 (R_0 / R)^6 \qquad (1\text{-}8)$$

where R_0 is the Förster radius, defined as the donor-acceptor separation corresponding to 50% of energy transfer, and k_F is the rate of excitation transfer when $R = R_0$. The donor-acceptor pair alone determines both k_F and R_0. The efficiency of energy transfer (E) is the fraction of photons absorbed by the donor that are transferred to the receptor. E is essentially the quantum yield of energy transfer, defined as follows:

$$E = N_1 / N_2 \qquad (1\text{-}9)$$

where N_1 is the number of quanta transferred from the donor to the acceptor and N_2 is number of quanta absorbed by the donor. E is also given by:

$$E = k(R) / [k_0 + k(R)] \qquad (1\text{-}10)$$

which is the ratio of the transfer rate to the total decay rate of the donor.

Then,

$$E = R_0^6 / (R_0^6 + R^6) \qquad (1\text{-}11)$$

This equation shows the strong dependence of the transfer efficiency of distance when the donor-acceptor distance is near R_0, which is determined by the following equation:

$$R_0^6 = (8.79 \times 10^{23}) \kappa^2 n^{-4} \Phi_d J_{da} \qquad (1\text{-}12)$$

in which Φ_d is the quantum efficiency of the donor probe attached to the molecule of interest; κ^2 is the Förster orientation factor, which can be 0-4, but is usually 2/3 if the orientation of the dipoles is random; n is the refractive index of the solvent (the value is 1.33-1.4); and J_{da} is the wavelength-dependent overlap of the donor spectrum with the

absorption spectrum of the acceptor. The unit of R_0 is Å, and its value is typically 10-50 Å. From the equation, R_0 can be calculated for a given FRET system.

FRET has proven to be a powerful spectroscopic technique to measure the distance in the 1-10 nm range [40-41]. Any changes in the donor and acceptor will result in a change in the transfer rate, allowing this technique to measure the distance between the sites upon the conformational change. It has been called "a spectroscopic ruler" [42]. Of the two kinds of fluorescence resonance energy transfer, heterotransfer is much more popular in the analysis of macromolecular interactions. It is widely used to determine distances in macromolecules between two or more different chromophores and thus to obtain structural information. Heterotransfer is observed between two different fluorescent dyes with different emission and adsorption spectra, resulting in a one-way transfer from donor to acceptor. The energy transfer efficiency can be measured by the change in the quantum field, the lifetime or polarization of the donor, or the enhancement of the acceptor. The energy is transferred in the Förster distance, and either steady state or time-resolved methods can be applied for the FRET measurements. It could be applied to study molecular interactions in membranes [43-45], protein structure and protein-protein interactions in solution [46-49], nucleic acids and nucleic acid-protein complexes [50-54], and immunoassays [55-56].

When FRET occurs in the same molecules in an identical environment (called homotransfer), the fluorescence intensity will not change. On the other hand, the polarization value may change due to the likely change of the fluorophores' orientation,

which results in depolarization [36]. This always happens to fluorophores with small Stoke's shifts. For the fluorescein-fluorescein pair, the calculated R_0 is 40 Å [57]; for BODIPY FL, it is 57 Å [58].

Homotransfer has been used to study protein structure [59], oligomerization [60-61], the organization of membrane proteins at cell surface [62-63], and protein conformational change [64]. It can only be monitored by FP, because the fluorescence intensity remains the same, rather than monitoring the intensity as in heterotransfer [65]. Homo-energy transfer leads to depolarization if the transition dipole moments of the two dyes are not parallel in the two subunits. Because the quantum yield of the fluorophore remains unchanged, the fluorescent lifetime is also constant. Depolarization due to homotransfer between multi-FAM fluorophores (up to four) has been used to study melittin oligomerizations [66]. In this study, homotransfer helps to measure the distance between the binding sites of protein.

1.4 Aptamers

Aptamers are artificial DNA or RNA oligomers that can bind to a given ligand with high affinity and specificity due to their particular structure, and therefore antagonize the biological function of the ligand [67-69]. They are obtained by systematic evolution of ligands by exponential enrichment (SELEX), a combinatorial chemistry methodology that allows nucleic acids generated from enormous libraries to recognize target molecules with high affinity and specificity and to identify protein signatures [70-73]. SELEX is a technique for screening very large combinatorial

libraries of oligonucleotides by a process of *in vitro* selection, partitioning, and PCR amplification [70] (Figure 1.4). The process of SELEX involves the synthesis of a library, selection or screening, and the structural analysis of the aptamer-target complex. After several (5 to 15) cycles of SELEX, single-stranded (ss) DNA or RNA aptamers can be obtained. They have high specificity and high affinity for the target molecules, usually 3 to 4 magnitudes higher than the starting library.

Aptamers are considered as substitutes of antibodies used in immunoassays [83]. Although aptamers mimic the properties of antibodies in a variety of diagnostic formats, they are different than antibodies. They can be used in molecular recognition, target identification and validation, and therapeutics. There are many advantages of using aptamers over antibodies for the identification and recognition of target proteins, because they avoid the problem of biopolymer denaturation during storage, are easier to produce, and are cheaper than antibodies. Aptamers are smaller and structurally simpler than antibodies, and they can be more easily reproduced because they can be synthesized *in vitro* chemically or by enzymatic methods, unlike antibodies, which can only be produced in living cells.

Aptamers usually have a size of 40-100 nucleotides, depending on the size of the region in the combinatorial DNA library, with affinity to the target molecule with a dissociation constant (K_d) at the nanomolar level. They not only bind to the targets efficiently, but can also recognize the tertiary structure of the targets. The information from aptamer-target binding will lead to the development of new aptamers, which can

SELEX Process

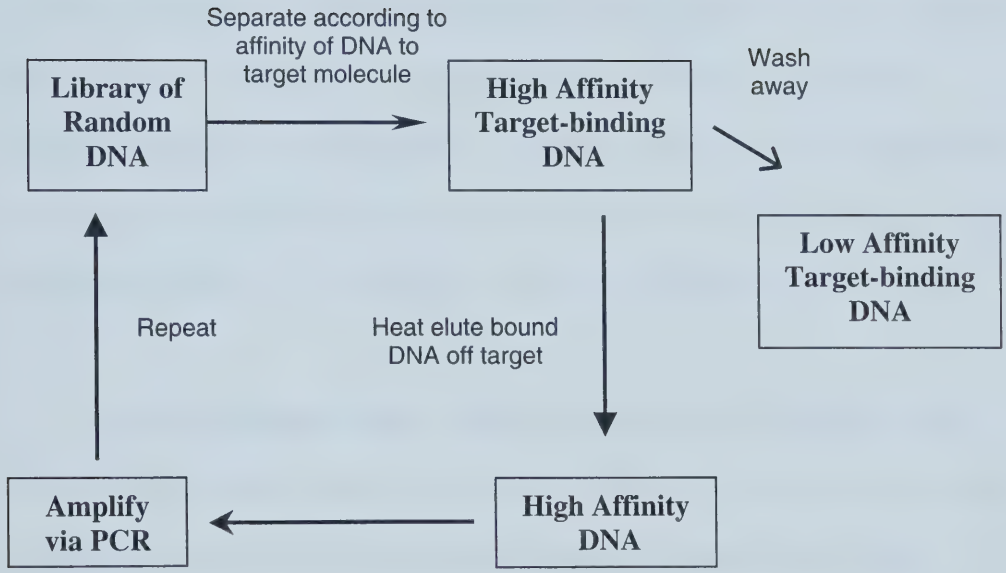

Figure 1.4 SELEX process

be modified by various hydrophobic, hydrophilic, or other reactive groups to enable construction of effective therapeutic agents [75-77]. Aptamers have been employed in diagnostic applications and have been used as affinity probes [54, 71, 78] and molecular beacons [79-81]. They have been applied in macro- and micro-arrays [72, 82], biosensors [83-84], and affinity chromatography to purify proteins [85].

Using a different starting library or partition method could select different aptamers that bind to different active sites of the protein. Research has shown that two different aptamers bind with thrombin at different sites [86-87]. Two identical aptamers were found to bind to the HIV-1 gag polyprotein at either the nucleocapsid or the matrix protein site [88]. Furthermore, DNA aptamers that were developed to inhibit the RNase H of HIV-1 RT were found to inhibit the HIV-1 integrase as well [89].

Studying the aptamer-target complex by means such as X-ray spectroscopy, NMR, or other indirect methods may be very informative, but the sensitivity can only reach the μM level. One RNA aptamer that formed complexes with its target molecule with different stoichiometries has been studied by ultracentrifugation and electrospray mass spectrometry [90].

Several DNA and RNA aptamers have been developed in recent years to bind to HIV-1 reverse transcriptase (RT) [67, 91-94]. RT12 is a single-stranded DNA aptamer that has been generated to bind specifically with the reverse transcriptase of the type 1 human immunodefiency virus (HIV-1) [91]. It is an 84-mer with a K_d of 2 nM, and was

originally designed to inhibit the activity of the RNA-dependent DNA polymerase of HIV-1 RT. RT26, an 81-mer, has a K_d of 1 nM with HIV-1 RT; RT1t49, a 49-mer, a shorter version of the aptamer, has a K_d of 4 nM with HIV-1 RT. ODN93, an 81-mer, has a K_d of 10 nM, and was initially selected to inhibit the activity of the RNase H site of HIV-1 RT [92]. A previous study has described the advantage of using an aptamer as a probe for the selective and direct determination of HIV-1 RT by CE/LIF [95]. However, stoichiometries between aptamers and the protein have not been investigated. The proposed secondary structure of the DNA aptamers, RT12, RT26 [96], and RT1t49 [91] are shown in Figure 1.5.

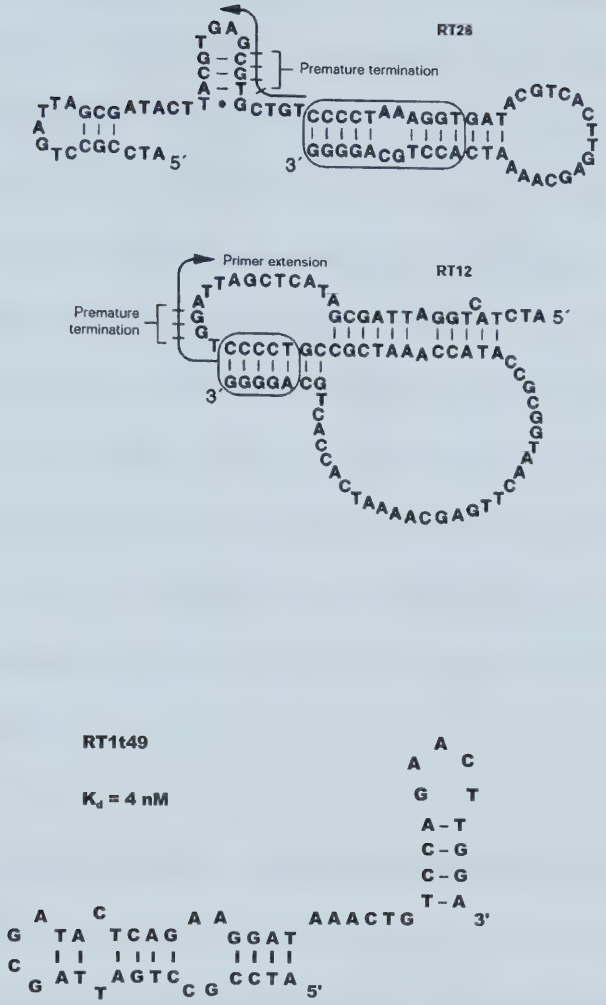

Figure 1.5 Proposed secondary structures of RT26, RT12, and RT1t49

1.5 HIV-1 RT

HIV-1 reverse transcriptase (HIV-1 RT) plays an essential role in the replication of the HIV-1 virus, the causative agent of AIDS [97-99]. It is responsible for the conversion of the ss-RNA of the HIV-1 virus into ds-DNA, which in turn is integrated into the host genome. HIV-1 RT is a multi-functional enzyme with RNA-dependent DNA polymerase, DNA-dependent DNA polymerase, and ribonuclease H (RNase H) activities. DNA polymerase is the enzyme that assembles the polymer from deoxyribonucleotides in the triphosphate form during DNA replication, and RNase H specifically cleaves the RNA in RNA:DNA hybrids during DNA replication. A major target for anti-HIV drugs, HIV-1 RT has been extensively studied since the 1980s. A considerable amount of information about the structure of HIV-1 RT from X-ray crystallography is available, of both the unbound HIV-1 RT and its complexes with various inhibitors, including ds-DNA, RNA-DNA template, and other binding molecules [100-108].

The HIV-1 RT enzyme consists of an asymmetric heterodimer of two subunits, p66 and p51. The activity of HIV-1 RT is confined only to its dimeric forms, and the most stable form is a heterodimer, p66/p51 [109-111]. p66/p51 is the only dimeric form *in vivo*; p66 represents a 66-kD subunit and p51 a 55-kD one. The p51 subunit is created from a p66 subunit when the RNase H is cleaved, and its sequence is identical to the N-terminal of p66. Both of them contain the regions necessary to catalyze the RNA-dependent DNA polymerization, but only p66 has the region necessary to catalyze the DNA-dependent DNA polymerization.

Figure 1.6 shows the structure of unliganded HIV-1 RT. The p66 subunit contains five subdomains [112-113]. It resembles a human's right hand, with fingers, thumb, palm, connection, and RNase H. The dimensions of p66 are approximately 100 × 30 × 45 Å, with these subdomains largely arranged side by side. There is a strong interaction between p66 and p51, while homodimers p66/p66 and p51/p51 show relatively low activity of HIV-1 RT. p51 is essential for the catalytic function of HIV-1 RT [114-115], but its activity is not clear. p51 has no cleft as has p66; it also has regions of palm, thumb, finger, and connection, but the polymerase site of p51 is buried under the palm of p66, and does not function in the heterodimer [100].

Because of the importance of reverse transcriptase in HIV replication, inhibitors of this enzyme are potential therapeutic agents in the battle against HIV [116]. There are two classes of RT inhibitors: the nucleoside RT inhibitors (NRTI) and the non-nucleoside RT inhibitors (NNRTI). NRTIs are the nucleotide and nucleoside analogs such as AZT, ddI, ddC, d4T, 3TC, and abacavir, whose dideoxy compounds lack a 3' oxygen, and which cause DNA chain termination when they are incorporated into a growing DNA strand. NNRTIs, such as nevirapine, delavirdine, and efavirenz, have been shown to bind to a hydrophobic pocket formed 10 Å away from the polymerase site. There is one inhibitor that can inhibit both the polymerase and the RNase H site at the same time [117]. Unfortunately, HIV RT develops point mutations quickly, resulting in drug resistance to nucleoside analog RT inhibitors, because HIV-1 RT is extremely tolerant of non-standard base pairs and modified ribose units,

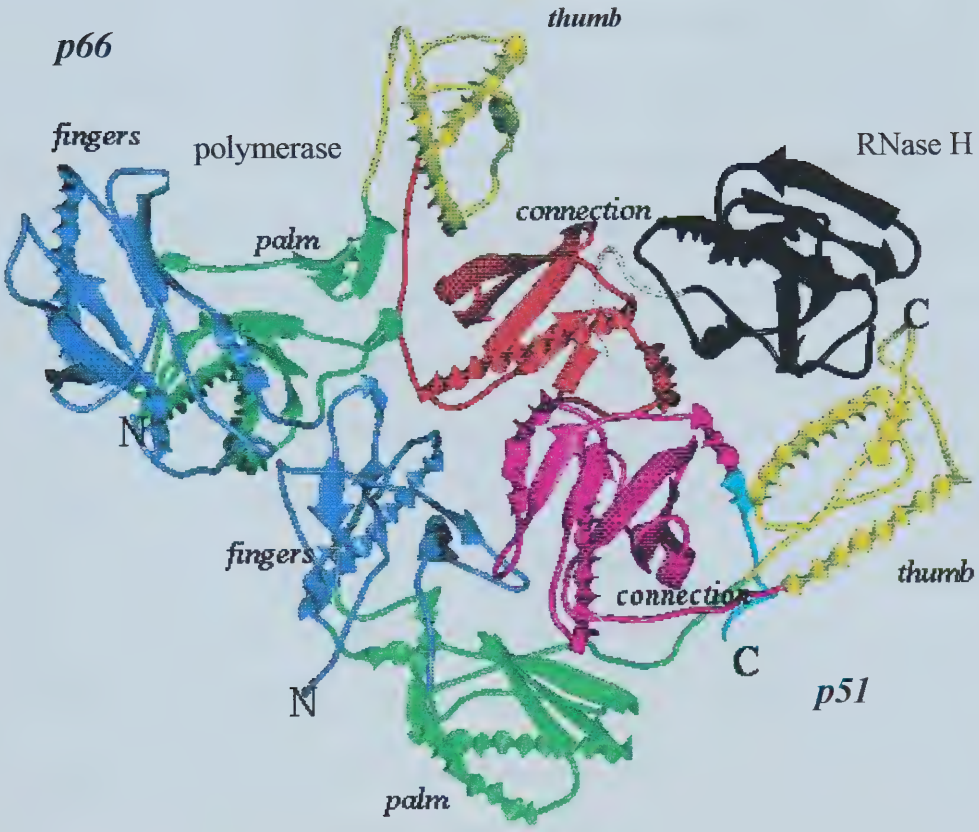

Figure 1.6 HIV-1 RT structure

leading to a high error rate of mutation on the HIV-1 genome. It shows high flexibility upon binding with various inhibitors [118].

HIV-1 RT can form a stable complex with both ds-DNA and ss-DNA, with no preferable specific sequences. This sets it apart from other DNA polymerases [119]. HIV-1 RT does not need auxiliary proteins to bind with DNA, and it binds with ds-DNA with higher affinity than ss-DNA. The polymerase site is mostly regarded as the binding site; however, the portions of RNase H containing amino acids have potential interactions with DNA. It is known that the DNA polymerase site and the RNase site of p66 overlap, when the polymerase site joins to the RNase H domain via a connection domain. These two active centers are separated by approximately 18 base pairs (bp) of DNA within a template-primer cleft, which is located at the palm domain of the p66 subunit [106, 120-124]. A template-primer ds DNA binds HIV-1 RT at a large cleft formed by the fingers, palm, and thumb of p66 (Figure 1.7). The DNA bends to fit into the p66 of HIV-1 RT to bind with the protein; this indicates that aptamers may have the proposed structure required to bind with the p66 subunit as well. This allows closer contact of the two binding sites while possibly binding with two ss-DNAs at the same time. Although HIV-1 RT is quite flexible upon binding with the substrate, the mechanism of how it recognizes DNA aptamers is unknown. Aptamers need to form suitable three-dimensional structures to be recognized by the target protein. The RNA aptamer binding with HIV-1 RT has been closely studied. It shows very close contact of the RNA and the cleft [125-126].

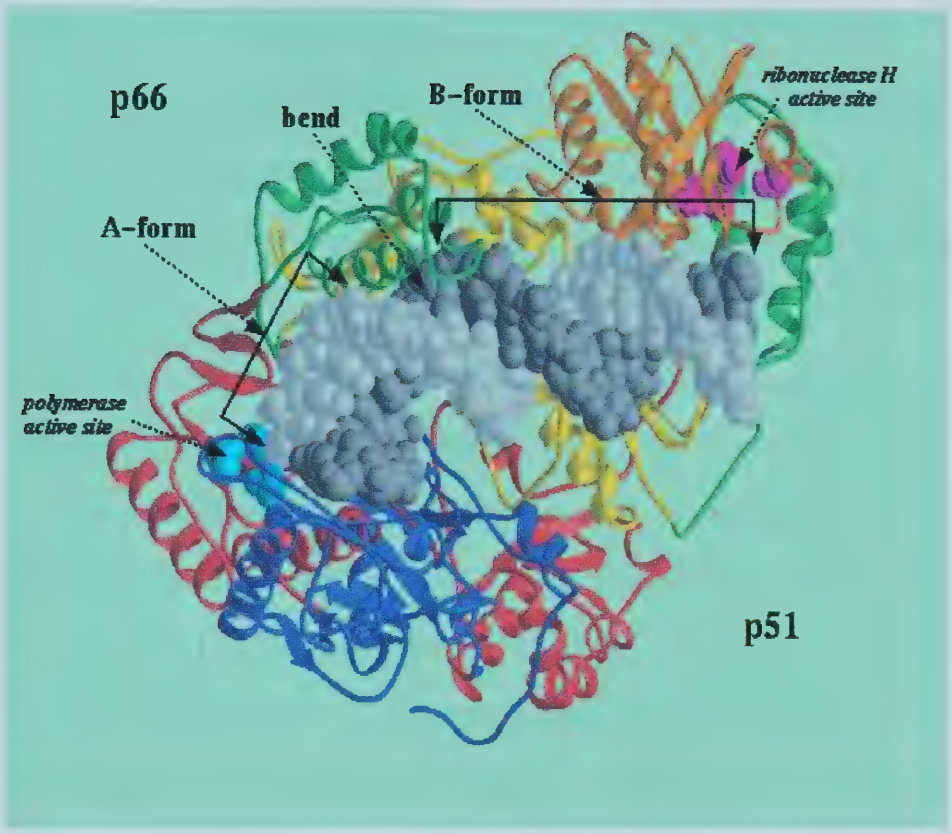

Figure 1.7 HIV-1 RT binding with ds-DNA

1.6 Thesis outline

The aims of the study were:

- to study the stoichiometries formed between HIV-1 RT and aptamers by ACE;
- to use FP to monitor the stoichiometries;
- to quantitate HIV-1 RT concentration by the methods developed in this study;
- to compare the affinities between HIV-1 RT and different aptamers;
- to study the effect of sample storage and denaturation on both DNA and protein.

The application of CE/LIF combined with FP to the analysis of the interactions between HIV-1 RT and DNA aptamers has demonstrated the partnership between the two techniques. In Chapter 2, CZE is used to separate the free aptamers from the complexes formed between aptamers and HIV-1 RT. Chapter 3 describes the studies of the stoichiometries of HIV-1 RT binding with aptamers using the FP technique. FP information suggests possible homo-FRET. Chapter 4 describes the effects of storage and denaturation on the formation of the complexes. Chapter 5 presents the quantitative determination of HIV-1 RT by CE/LIF using RT12 as a probe.

1.6 References

1. Landers, J.P.; (ed.) *Handbook of Capillary Electrophoresis* CRC Press, New York, **1997**
2. Khaledi, M.G. (ed.) *High-Performance Capillary Electrophoresis: Theory, techniques, and applications* John Wiley & Sons, New York, **1998**
3. Altria, K.D. *J. Chromatogr. A* **1999**, 856, 443-463
   Overview of capillary electrophoresis and capillary electrochromatography
4. Weinberger, R. *Practical Capillary Electrophoresis* Academic Press, San Diego, **2000**
5. Camilleri, P. (ed.) *Capillary Electrophoresis Theory and Practice* CRC Press, Boca Raton, Fla., **1993**
6. Hu, S.; Dovichi, N.J. *Anal. Chem.* **2002**, 74, 2833-2850
   Capillary Electrophoresis for the Analysis of Biopolymers
7. Melanson, J.E.; Baryla, N. E.; Lucy, C.A. *Trends Anal. Chem.* **2001**, 20, 365-374
   Dynamic Capillary Coatings for Electroosmotic Flow Control in Capillary Electrophoresis
8. Bello, M.S.; Capelli, L.; Righrtti, P. G. *J. Chromatogr. A.* **1994**, 684, 311- 322
   Dependence of the electroosmotic mobility on the applied electric field and its reproducibility in capillary electrophoresis
9. Corradini, D. *J. Chromatogr. B* **1997**, 699, 221-256
   Buffer additives other than the surfactant sodium dodecyl sulfate for protein separations by capillary electrophoresis
10. Huang, T.L.; Tsai, P.; Wu, C.T.; Lee, C.S. *Anal. Chem.* **1993**, 65, 2887- 2893
    Mechanistic studies of electroosmotic control at the capillary-solution interface
11. Lambert, W.J.; Middleton, D.L. *Anal. Chem.* **1990**, 62, 1585-1587
    pH hysteresis effect with silica capillaries in capillary zone electrophoresis
12. Schwer, C.; Kenndler, E. *Anal. Chem.* **1991**, 63, 1801-1807
    Electrophoresis in fused-silica capillaries: the influence of organic solvents on the electroosmotic velocity and the .zeta. potential
13. Chen, D.Y.; Dovichi, N.J. *Anal. Chem.* **1996**, 68, 690-696

Single-molecule detection in capillary electrophoresis: molecular shot noise as a fundamental limit to chemical analysis

14. Rippel, G.; Gorstjen, H.; Billiet, H.A.H.; Frank, J. *Electrophoresis* **1997,** 18, 2175-2183

Affinity capillary electrophoresis

15. Chu, Y. -H.; Avila, L.Z.; et al *Acc. Chem. Res.* **1995**, 28, 461-468

Affinity capillary electrophoresis

16. Lausch, R.; Reif, O. -W.; Riechel, P.; Scheper, T. *Electrophoresis* **1995**, 16, 636-641

Analysis of IgG using a capillary electrophoretic affinity assay with protein A and laser-induced fluorescence detection

17. Kelly, J.A.; Reddy, R.; Lee, C.S. *Anal. Chem.* **1997**, 69, 5152-5158

Mechanistic Studies of Postcapillary Affinity Detection for Capillary Zone Electrophoresis Based on the Biotin-Streptavidin System

18. Chiem, N.; Harrison, D. J. *Anal. Chem.* **1997**, 69, 373-378

Microchip-Based Capillary Electrophoresis for Immunoassays: Analysis of Monoclonal Antibodies and Theophylline

19. Okun, V.M.; Ronacher, B.; Blaas, D.; Kenndler, E. *Anal. Chem.* **2000**, 72, 4634 – 4639

Affinity Capillary Electrophoresis for the Assessment of Complex Formation between Viruses and Monoclonal Antibodies

20. Krylov, S.N.; Dovichi, N. J. *Anal. Chem.* **2000**, 72, 111R-128R

Annul Review of Capillary electrophoresis

21. Korf, G.M.; Landers, J.P.; O'kane, D.J. *Anal. Chem.* **1997**, 251, 210-218

Capillary Electrophoresis with Laser-Induced Fluorescence Detection for the Analysis of Free and Immune-Complexed Green Fluorescent Protein

22. Heegaard, N. H.H. *J. Mol. Recognit.* **1998**, 11, 141-148

Capillary electrophoresis for the study of affinity interactions

23. Duijn, R.M.G.; Frank, J.; van Dedem, G.W.K.; Baltussen, E. *Electrophoresis*, **2000**, 21, 3905-3918

Recent advances in affinity capillary electrophoresis

24. Heegaard, N.H.H.; Kennedy, R.T. *Electrophoresis* **1999**, 20, 3122-3133

Identification, quantitation, and characterization of biomolecules by capillary electrophoretic analysis of binding interactions

25. Tseng, W. -L.; Chang, H.T.; et al *Electrophoresis* **2002**, 23, 836-846
Immunoaffinity capillary electrophoresis: Determination of binding constant and stoichiometry for antibody-antigen interaction

26. Chu, Y.-H.; Cheng,C.C. *Cell. Mol. Life Sci.* **1998**, 54, 663-683
Affinity capillary electrophoresis in biomolecular recognition

27. Lakowicz, J.R. *Principles of Fluorescence Spectroscopy* Kluwer Academic/Plenum Press, New York, **1999**

28. Rendell, D. *Fluorescence and phosphorescence Spectroscopy* Wiley, London, **1987**

29. Perin, F. *Journal de physique et le Radium* **1926**, 7, 390-401
Polarisation de la Lumiere de Fluorescence. Vie Moyenne des Molecule dans L'etat excite

30. Weber, G. *Adv. Protein. Chem.* **1953**, 8, 415-459
Rotational Brownian motion and polarization of the fluorescence solutions

31. Prystay, L.; Gosselin, M.; Banks P. *J. Biomol. Screening* **2001**, 6, 141-150
Determination of equilibrium dissociation constants in fluorescence polarization

32. Lundblad, J.R.; Laurance, M.; Goodman, R.H. *Mol. Endocrinol.* **1996**, 10, 607-612
Fluorescence polarization analysis of protein-DNA and protein-protein interactions.

33. Ladokhin, A.S. **Fluorescence Spectroscopy in Peptide and Protein Analysis**, in *The Encyclopedia of Analytical Chemistry,* 5762-5779, Jon Wiley & Sons Ltd, Chichester, **2000**

34. Lentz, B.R. *Chem. Phys. Lipids* **1993**, 64, 99-116
Use of fluorescent probes to monitor molecular order and motions within liposome bilayers."

35. Dandliker, W.B.; Feigen, G.A. *Biochem. Biophys. Res. Commun.* **1961**, 5, 299-304.
Quantification of antigen-antibody by the fluorescence polarization

36. Weber, G. *Trans. Faraday Soc.* **1954**, 50, 552-555
Dependence of the polarization of the fluorescence of the concentration

37. Cantor, C.R.; Schimmel, P.R. *Biophysical Chemistry* Freeman, W. H. and Company, San Francisco, **1980**

38. Perrin, F. *Ann. Phys. Paris.* **1929**, 12, 169-175.
La fluorescence des solutions

39. Demidov, A.A.; Andrews, D.L. **Polarization in Molecular Complexes with Incoherent Energy Transfer** in *Resonance Energy Transfer* (Ed.) Andrews, D.L.; Demidov, A.A. Wiley, Chichester, **1999**, 435-465

40. Wu, P.; Brand, L. *Anal. Biochem.* **1994**, 218, 1-13
Resonance Energy Transfer: Methods and Applications

41. Clegg, R.M. *Cur. Opin. Biotechnol.* **1995**, 6,103-110
Fluorescence Resonance Energy Transfer

42. Stryer, L.; Haugland, R. P. *PNAS USA* **1967**, 58, 719-726
Energy transfer: a spectroscopic ruler

43. Bettio, A.; Beck-Sickinger, A.G. *Biopolymers* **2001**, 60, 420-437
Biophysical methods to study ligand-receptor interactions of neuropeptide Y

44. Eisenhawer, M.; Cattarinussi, S.; Kuhn, A.; Vogel, H. *Biochemistry* **2001**, 40, 12321-12328
Fluorescence resonance energy transfer shows a close helix-helix distance in the transmembrane M13 procoat protein

45. Kakehi, K.; Oda, Y.; Kinoshita, M. *Anal. Biochem.* **2001**, 29, 111-116
Fluorescence Polarization: Analysis of Carbohydrate–Protein Interaction

46. Overton, M. C.; Blumer, K.J. *Methods* **2002**, 27, 324-332
Use of fluorescence resonance energy transfer to analyze oligomerization of G-protein-coupled receptors expressed in yeast

47. Scheibner, K.A.; Zhang, Z.; Cole, P. A. *Anal. Biochem.* **2003**, 317, 226-232
Merging fluorescence resonance energy transfer and expressed protein ligation to analyze protein–protein interactions

48. Miki, M.; Kouyama, T. *Biochemistry* **1994**, 33, 10171-10177
Domain Motion in Actin Observed by Fluorescence Resonance Energy Transfer

49. Banks, P.; Harvey, M. *J. Biomol. Screen* **2002**, 7, 111-117
Considerations for using fluorescence polarization in the screening of g protein-coupled receptors

50. Lorenz, M.; Hillisch, A.; Diekmann, S. *Curr. Opin. Struct. Biol.* **2001**, 11, 201-207
Recent advances in FRET: distance determination in protein–DNA complexes

51. Stühmeier, F.; Hillisch, A.; Clegg, R.M.; Diekmann, S. *J. Mol. Biol.* **2000**, 302, 1081-1100

Fluorescence Energy Transfer Analysis of DNA Structures Containing Several Bulges and their Interaction with CAP

52. Yang, M. S.; Ghosh, S. S.; Millar, D. P. *Biochemistry* **1994,** 33, 15329-15337
Direct Measurement of Thermodynamic and Kinetic Parameters of DNA Triple Helix Formation by Fluorescence Spectroscopy

53. Lilley, D.M.J.; Wilson, T.J. *Curr. Opin. Biotechnol.* **2000**, 4, 507-517
Fluorescence resonance energy transfer as a structural tool for nucleic acids

54. Kido, C.; Murano, S.; Tsuruoka, M. *Gene* **2000**, 259, 123-127
Rapid and simple detection of PCR product DNA: a comparison between Southern hybridization and fluorescence polarization analysis

55. Szollosi, J.; Damjanovich, S.; Matyus, L. *Cytometry* **1998**, 34, 159-179
Application of fluorescence resonance energy transfer in the clinical laboratory: Routine and research

56. Malecki, M.; Hsu, A.; Truong, L.; Sanchez, S. *PNAS USA* **2002**, 99, 213-218
Molecular immunolabeling with recombinant single-chain variable fragment (scFv) antibodies designed with metal-binding domains

57. Hamman, B. D.; Oleinikov, A. V.; Jokhadze; G. G.; Traut, R. R.; Jameson, D. M. *Biochemistry* **1996**, 35, 16672-16679
Rotational and Conformational Dynamics of *Escherichia coli* Ribosomal Protein L7/L12

58. Johnson, I.D.; Kang, H.C.; Haugland, R.P. *Anal. Biochem.* **1991**, 198, 228-237
Fluorescent membrane probes incorporating dipyrrometheneboron difluoride fluorophores

59. Bastiaens, P. I. H.; van Hoek, A; et al *Biophys. J.* **1992**, 63, 839-853
Conformational dynamics and intersubunit energy transfer in wild-type and mutant lipoamide dehydrogenase from *Azotobacter vinelandii*: a multidimensional time-resolved polarized fluorescence study

60. Runnels, L. W.; Scarlata, S.F. *Biophys. J.* **1995**, 69,1569-1583
Theory and application of fluorescence homotransfer to melittin oligomerization

61. Blackman, S. M.; Piston, D.W.; Beth, A.H. *Biophys. J.* **1998**, 75,1117-1130
Oligomeric state of human erythrocyte band 3 measured by fluorescence resonance energy homotransfer

62. Varma, R.; Mayor, S. *Nature* **1998**, 394, 798-801
GPI-anchored proteins are organized in submicron domains at the cell surface.

63. Gautier, I.; Tramier, M.; et al *Biophys J.* **2001**, 80, 3000-3008

Homo-FRET Microscopy in Living Cells to Measure Monomer-Dimer Transition of GFP-Tagged Proteins

64. Heyduk, T. *Curr. Opin. Biotechnol.* **2002**, 13, 292-296
Measuring protein conformational changes by FRET/LRET

65. Van der Meer, B. W.; Coker, G. III; Chen, S.-Y. *Resonance Energy Transfer: Theory and Data* VCH Publishers, New York, **1994**

66. Sjoback, R.; Nygren, J.; Kubista M *Biopolymers* **1998**, 46, 445-453
Characterization of fluorescein-oligonucleotide conjugates and measurement of local electrostatic potential

67. Turek, C.; Gold, L. *Science* **1990**, 249, 505-510
Systematic Evolution of Ligands by Exponential Enrichment: RNA Ligands to Bacteriophage T4 DNA Polymerase

68. Ellington, A. D.; Szostak, J. W. *Nature* **1990**, 346, 818-822
In vitro selection of RNA molecules that bind specific ligands

69. Joyce, G. F. *Gene* **1989**, 82, 83-87
Amplification, mutation and selection of catalytic RNA

70. James, W. **Aptamers**. In *The Encyclopedia of Analytical Chemistry: Instrumentation and applications*, 4848-4871, Jon Wiley & Sons Ltd, Chichester, **2000**

71. Kotia, R. B.; Li, L.; McGowan, L. B. *Anal. Chem.* **2000**, 72, 827-831.
Separation of Nontarget Compounds by DNA Aptamers

72. Petach, H.; Gold, L. *Curr. Opin. Biotechnol.* **2002**, 13, 309-314.
Dimensionality is the issue: use of photoaptamers in protein microarrays

73. Romig T.S.; Bell, C.; Drolet, D.W. *J. Chromatogr. B.* **1999**, 731, 275-284.
Aptamer affinity chromatography:: combinatorial chemistry applied to protein purification

74. Jayasena, S.D. *Clin. Chem.* **1999**, 45, 1628-1650
Aptamers: An Emerging Class of Molecules That rival Antibodies in Diagnostics

75. Gold, L. *J. Biol. Chem.* **1995**, 270, 13581-13584
Oligonucleotides as Research, Diagnostic,and Therapeutic Agents

76. Eaton, B.E.; Gold, L.; et al *Bioorg. Med. Chem.* **1997**, 5, 1087-1096
Post-SELEX Combinatorial Optimization of Aptamers.

77. Osborne, S.E.; Matsumura, I.; Ellington, A. D. *Curr. Opin. Chem. Biol.* **1997**, 1, 5-9

Aptamers as therapeutic and diagnostic reagents: problems and prospects

78. Hesselberth, J.; Robertson, M.P.; Jhaveri, S.; Ellington, A. D. *J. Biotechnol.* **2000**, 74, 15-25

In vitro selection of nucleic acids for diagnostic applications

79. Hamaguchi, N., Ellington, A., Stanton, M. *Anal. Biochem.* **2001,** 294, 126-131

Aptamer Beacons for the Direct Detection of Proteins

80. Yamamoto, R.; Baba, T.; Kumar, P.K. *Genes Cells* **2000**, 5, 389-396

Molecular beacon aptamer fluoresces in the presence of Tat protein of HIV-1

81. Li, J.W.; Fang, X.H.; Tan, W.H. *Biochem. Biophys. Res. Commun.* **2002**, 292, 31-40

Molecular aptamer beacons for real-time protein recognition

82. Lopez, M.F.; Pulskal, M.G. *J. Chromatogr. B* **2003**, 787, 19-27

Protein Micro- and Macroarrays: Digitizing the Proteome

83. O'Sullivan, C.K. *Anal. Bioanal. Chem.* **2002**, 372, 44-48

Aptasensors-the future of biosensing

84. Stojanovic, M. N.; de Prada, P.; Landry, D. W. *J. Am. Chem. Soc.* **2000**, 122, 11547-11548

Fluorescent Sensors Based on Aptamer Self-Assembly

85. Gadgil, H.; Oak, S. A.; Jarrett, H.W. *J. Biochem. Biophys. Methods* **2001**, 49, 607-624

Affinity Purification of DNA-binding proteins

86. Tasset, D. M.; Kubik, M.F.; Steiner, W. *J. Mol. Biol.* **1997**, 272, 688-698

Oligonucleotide inhibitors of human thrombin that bind distinct epitopes

87. Bock, L.C.; Griffin, L.C.; Latham, J.A.; Vermaas, E.H.; Toole, J.J. *Nature* **1992**, 355, 564-566

Selection of single-stranded DNA molecules that bind and inhibit human thrombin

88. Lochrie, M.A.; Waugh, Sheela; et al *Nucleic Acids Rec.* **1997**, 25, 2902-2910

In vitro Selection of RNAs that bind to the HIV-1 gag polyprotein

89. De Soultrait, V.R.; Lozach, P.-Y.; Altmeyer, R.; Tarrago-Litvak, L.; Litvak, S.; Andreola, M.L. *J. Mol. Biol.* **2002**, 324, 195-203

DNA aptamers derived from HIV-1 RNase H inhibitors are strong anti-integrase agents

90. Cassiday, L.A.; Lebruska, L.L.; et al *Anal. Biochem.* **2002**, 306, 290-297

Binding Stoichiometry of an RNA Aptamer and Its Transcription Factor Target

91. Schneider, D. J.; Feignon, J.; Hostomsky, Z.; Gold, L. *Biochemistry* **1995**, 34, 9599-9610

High-affinity ssDNA inhibitors of the reverse transcriptase of type 1 human immunodeficiency virus

92. Andreola, M. L.; Pileur, F.; Calmels, C.; Ventura, M.; Tarrago-Litvak, L.; Toulme, J. J.; Litvak, S. *Biochemistry* **2001**, 40, 10087-10094.

DNA Aptamers Selected against the HIV-1 RNase H Display *in Vitro* Antiviral Activity

93. Joshi, P.; Prasad., V.R. *J. of Virol.* **2002**, 76, 6545-6557

Potent inhibition of human immunodeficiency virus type 1 replication by template analog reverse transcriptase inhibitors derived by SELEX (systematic evolution of ligands by exponential enrichment

94. Tuerk, C.; Macdougal, S.; Gold, L. *PNAS USA* **1992**, 89, 6988–6992

RNA pseudoknots that inhibit human immunodeficiency virus type-1 reverse transcriptase

95. Pavski, V.; Le, X.C. *Anal. Chem.* **2001**, 73, 6070 – 6076

Detection of Human Immunodeficiency Virus Type 1 Reverse Transcriptase Using Aptamers as Probes in Affinity Capillary Electrophoresis

96. Breaker, R.R. *Curr. Opin. Chem. Biol.* **1997**, 1, 26-31

DNA aptamers and DNA enzymes

97. Telesnitsky, A.; Goff, S.P. *Reverse transcriptase and the generation of retroviral DNA*. In *Retrovirus* Coffin, J.M.; Hughes, S.H.; Varmus, H.E. (eds) Cold Spring Harbor Laboratory Press, Cold Spring Harbor, NY, **1997**

98. Skalka, A.; Goff, Stephen (ed.). *Reverse Transcriptase* Cold Spring Harbor Laboratory Press, **1993**, NY

99. Turner, B.G.; Summers, M.F. *J. Mol. Biol.* **1999**, 285, 1-32

Structural Biology of HIV

100. Jacobo-Molina, A.; Ding, J.; et al *PNAS USA* **1993**, 90, 6320-6324

Crystal Structure of HIV-1 RT complexed with ds-DNA at 3.0 Å resolution shows bent DNA

101. Hsiou, Y.; Ding, J.; et al *Structure*, **1996**, 4, 853-860

Structure of unliganded HIV-1 RT at 2.7 Å resolution: implication of conformational changes for polymerization and inhibition mechanisms

102. Rodgers, D.W; Gamblin, S.J.; et al *PNAS USA* **1995**, 92,1222-1226

The structure of unliganded reverse transcriptase from the human immunodeficiency virus type 1

103. Davis, J.F.; Hostomska, Z.; et al *Science* **1991**, 252, 88-95

Crystal structure of the ribonuclease H domain of HIV-1 RT

104. Ding, J.; Hughes, S.H.; Arnold, E. *Biopolymers* **1997**, 44, 125–138.

Protein–nucleic acid interactions and DNA conformation in a complex of HIV-1 RT with a double-stranded DNA template-primer

105. Sarafianos, S. G.; Das, K.; et al *EMBO J.* **2001**, 20, 1449-1461

Crystal structure of HIV-1 reverse transcriptase in complex with a polypurine tract RNA:DNA

106. Huang, H.; Chopra, R.; Verdine, G.L.; Harrison, S.C. *Science* **1998**, 282, 1669–1675

Structure of a covalently trapped catalytic complex of HIV-1 RT: implications for drug resistance

107. Ding, J.; Das, K.; Hsiou, Y.; et al *J. Mol. Biol.* **1998**, 284, 1095–1111

Structure and functional implications of the polymerase active site region in a complex of HIV-1 RT with double-stranded DNA and an antibody Fab fragment at 2.8 Å resolution

108. Kohlstaedt, L.A.; Wang, J.; Friedman, J.M.; Rice, P.A.; Steitz, T.A *Science* **1992**, 256, 1783–1790

Crystal structure at 3.5 Å resolution of HIV-1 RT complexed with an inhibitor

109. Restle, T.; Müller, B.; Goody, R.S. *J. Biol. Chem.* **1990**, 265, 8986-8988

Dimerization of HIV-1 RT dimeric forms

110. Restle, T.; Müller, B.; Goody, R.S. *FEBS Lett.* **1992**, 300, 97-100

RNase H activity of HIV RT is confined exclusively to dimeric forms

111. Lebowitz, J.; Kar, S.; et al *Protein Science* **1994**, 3, 1374-1382

HIV-1 RT heterodimer stability

112. Madrid, M.; Jacobo-Molina, A.; Ding, J.; Arnold, E. *Proteins* **1999,** 35, 332-337

Major subdomain rearrangement in HIV-1 reverse transcriptase simulated by molecular dynamics

113. Jonckheere, H.; De Vreese, K.; et al. *J. Virol. Methods* **1996**, 61, 113-125

Functionality of the subunits of the reverse transcriptase of the human immunodeficiency virus type I

114. Harris, D.; Lee, R.; et al *Biochemistry* **1998**, 37, 5903-5908

The p51 subunit of HIV-1 RT is essential in loading the p66 subunit on the template primer

115. Tasara, T.; Amacker, M.; Hubscher, U. *Biochemistry* **1999**, 38, 1633-1642
Intramolecular chimeras of the p51 subunit between HIV-1 and FIV RT suggest a stabilizing function for the p66 subunit in the heterodimeric enzyme

116. Jonckheere, H; Snne, J.; De Clercq; E. H. *Med. Res. Rev.* **2000**, 20, 129-154
The HIV-1 RT process as Target for RT inhibitors

117. Borkow, G.; Fletcher, R. S.; Barnard, J.; Arion, D.; Motakis, D.; Dmitrienko, G. I.; Parniak, M. A.; *Biochemistry* **1997**, 36, 3179-3185
Inhibition of the Ribonuclease H and DNA Polymerase Activities of HIV-1 Reverse Transcriptase by *N*-(4-*tert*-Butylbenzoyl)-2-hydroxy-1-naphthaldehyde Hydrazone

118. Madrid, M.; Lukin, J. A.; Madura, J.D.; Ding, J.; Arnold, E. *Proteins* **2001**, 45,176-182
Molecular dynamics of HIV-1 reverse transcriptase indicates increased flexibility upon DNA binding

119. Bakhanashvili, M.; Hizi, A. *Biochemistry* **1994**, 33, 12222-12228
Interaction of the reverse transcriptase of human immunodeficiency virus type 1 with DNA

120. Wöhrl, B. M.; Moelling, K. *Biochemistry* **1990**, 29, 10141–10147
Interaction of HIV-1 RNase H with polypurine tract containing RNA-DNA hybrids

121. Gopalakrishnan, V.; Peliska, J. A.; Benkovic, S.J. *PNAS USA* **1992**, 89, 10763–10767
HIV-1 RT: Spatial and temporal relationship between the polymerase and RNase H activities

122. Gao, H. Q.; Boyer, P.L.; Arnold, E.; Hughes, S. H. *J. Mol. Biol.* **1998**, 277, 559–572
Effects of mutations in the polymerase domain on the polymerase, RNase H and strand transfer activities of HIV-1 RT

123. Gao, H.Q.; Sarafianos, S.G.; Arnold, E.; Hughes, S.H. *J. Mol. Biol.* **1999**, 294, 1097–1113
Similarities and differences in the RNase H activities of HIV-1 RT and Moloney murine leukemia virus RT

124. Götte, M.; Maier, G.; Gross, H.J.; Heumann, H. *J. Biol. Chem.* **1998**, 273, 10139–10146

Localization of the active site of HIV-1 RT-associated RNase H domain on a DNA template using site-specific generated hydroxyl radicals.

125. Kensch, O.; Connolly, B.A.; et al *J. Biol. Chem.* **2000**, 275, 18271 - 18278. **HIV-1 Reverse Transcriptase-Pseudoknot RNA Aptamer Interaction Has a Binding Affinity in the Low Picomolar Range Coupled with High Specificity**

126. Jaeger, J.; Restle, T.; Steitz, T.A. *EMBO J.* **1998**, 17, 4535-4542 **The structure of HIV-1 reverse transcriptase complexed with an RNA pseudoknot inhibitor**

Chapter 2 CE/LIF Study of Aptamers Binding with HIV-1 RT

2.1 Introduction

2.1.1 HIV-1 Reverse Transcriptase and Aptamers

HIV reverse transcriptase (HIV RT) is a key enzyme of the retroviral life cycle; it catalyzes the conversion of the single-stranded genomic viral RNA into double-stranded DNA, which in turn is integrated into the host genome [1-3]. It is responsible for RNA-dependent DNA polymerization, RNase H activity, and DNA-dependent DNA polymerization. The enzyme consists of an asymmetric heterodimer of two subunits, p66 (66 kDa) and p51 (51 kDa), and is only active as a dimer [3]. The p66 subunit has both the DNA polymerase and the RNase H active domains, while the RNase H domain at the p51 subunit has been cleaved. Although the p51 and p66 subunits share 450 amino acids, and the polymerase domains of p66 and p51 each contain four domains with fingers, palm, thumb, and connection, their relative arrangements are significantly different [4]. Research shows that HIV-1 RT binds with a 19-base/18-base double-stranded DNA at the polymerase and extension to RNase H active sites at p66, while p51 shows no catalytic function during the polymerase process, because the polymerase site of p51, the palm region, is blocked by the connection domain [5]. The DNA polymerase site and the RNase site of p66 are overlapping, probably 60Å away from each other [6-7].

DNA aptamers RT26, RT12, RT1t49 and ODN93 have been selected as polymerase inhibitors of HIV-1 RT [8-9]. Pavski and Le have developed an assay that

uses RT26 as a probe to detect HIV-1 RT in solution [10]. However, the binding stoichiometries of DNA aptamers and HIV-1 RT have not been studied. No X-ray crystallographic information of how DNA aptamers bind with reverse transcriptase is available. RT12 and RT26 are inhibitors of HIV-1 RT, and have the same structure of 3'-GGGG and internal CCCC that mimics the primer:template junction. RT1t49 is a shorter aptamer; it lacks 3'-GGGG and has no internal CCCC part [8]. ODN93 has a G-rich part that adopts a G-quartet structure, which is probably essential for binding with the RNase H site [9]. ODN93 shows activities that inhibit the DNA polymerase as well [9]. HIV-1 RT has a large surface of interaction with nucleic acids. It may provide more than one non-specific binding site with single-stranded DNA after specific binding with its active sites. However, the affinity for such non-specific binding is much lower.

2.1.2 Affinity Capillary Electrophoresis and Laser-induced Fluorescence

Affinity capillary electrophoresis (ACE) is a useful tool for studies of interactions of biomolecules [11-13]. ACE combines the specificity of antibodies with the speed and resolving power of capillary electrophoresis. It is based on the measurement of the changes in the mobility of the substrate (or ligand) in a protein-ligand binding pair as a function of the concentration of the other partner (e.g. protein). Combined with laser-induced fluorescence, this method is highly sensitive.

Several methods, such as analytical ultra-centrifugation [14], electrospray mass spectrometry [15], and calorimetry [16] have been employed to study RNA aptamer

binding stoichiometry. The combination of CE/LIF and FP can potentially provide direct evidence of stoichiometries as well as structural information with less time and labor and higher sensitivity.

This chapter describes the use of several aptamers, RT12, RT26, RT1t49, and ODN93, to study the stoichiometries of aptamer binding with HIV-1 RT by CE/LIF. Two complexes were formed between HIV-1 RT and each of RT12, RT26, and ODN93, and were separated from free aptamers by CE. Only one complex formed with the shortest aptamer RT1t49.

2.2 Experimental

2.2.1 Reagents

All solutions were prepared with 18.2 MΩ distilled, deionized water (DDW) from a Milli-Q Gradient 10 Water System (Millipore, Nepean, ON, Canada). Tris-borate-EDTA (TBE) (0.089 M Tris, 0.089 M boric acid, 0.0025 M EDTA, pH 8.3) and Tris-glycine (0.025 M Tris, 0.192 M glycine, pH 8.3) were prepared with reagent-grade materials diluted to desirable concentrations with DDW prior to being filtered through a 0.22 μm filter to remove any particulate matter. The BODIPY®-FL dye, at 10^{-7} M (Molecular Probes, Eugene, OR, USA) was used for instrument alignment. The RT12 aptamer, an 84-mer with a sequence of (5′-ATCTACTGGATTAGCGATACTCGAT-TAGGTCCCCTGCCGCTAAACCATACCGCGGTAACTTGAGCAAAATCACCA-CTGCAGGGG-3′, RT26, an 81-mer with a sequence of (5'-ATCCGCCTGATTAGC-GATACTTA-CGTGAGCGTGCTGTCCCCTAAAGGTGATACGTCACTTGAGCA-

AAATCACCT-GCAGGGG-3'), RT1t49, an 49-mer with a sequence of (5'-ATCCGC-CTGATTAGCGATACTCAGAAGGATAAACTGTCCAGAACTTGGA-3'), and ODN93, an 81-mer with a sequence of (5'-CCCCTGCAGGTGATTTTGCTCAAGT-GGGGGTGGGAGGAGGTAGGCCTTAGGTTTCTGAAGTATCTCGAATCAGGC-GGAATA-3') were synthesized and labeled with 5′-FAM (5′-carboxyfluorescein) by University Core DNA Services (University of Calgary, Calgary, AB, Canada). HIV-1 RT was supplied by Worthington Biochemicals (Lake Wood, NJ, USA).

2.2.2 Stock solutions

The aptamers were diluted to 100 μL in 1× TBE (Tris-borate-EDTA) in 1000 μL micro-centrifuge tubes containing aptamers at 80 nM. They were stored at -20°C when not in use. A stock solution of HIV-1 RT was diluted to 1000 nM in DDW (deionized distilled water). Aliquots of HIV-1 RT solutions were stored at -20°C when not in use.

The aptamer and HIV-1 RT were added to the desired concentrations by pipeting the appropriate volumes of the stock solutions to make a final volume of 60 μL volume in a 200 μL microcentrifuge tube. The mixture was incubated for 3-5 min, and then an aliquot was injected into the capillary for analysis.

2.2.3 Instrument

A laboratory-built CE/LIFP instrument used in this work has been previously described [17-19] (Figure 2.1). The system consists of a high-voltage CE power supply

(model CZE 100R, Spellman, Plainview, NY, USA) and an uncoated fused-silica capillary (20 μm i.d., 150 μm od., Polymicro Technologies, Phoenix, AZ, USA); the latter was cut to 40 cm (later to 25 cm for faster separation) and inserted into the sheath flow cuvette (NSG Precision Cells, Farmingdale, NY, USA). The vertically-polarized laser beam (500:1) from an Argon ion laser (model 2144-65ML, Uniphase, San Jose, CA, USA) was filtered through a laser line filter (480 nm, 10 nm bandwidth, Newport, Fountain Valley, CA, USA) and focused to a detection window near the end of the tip of the capillary.

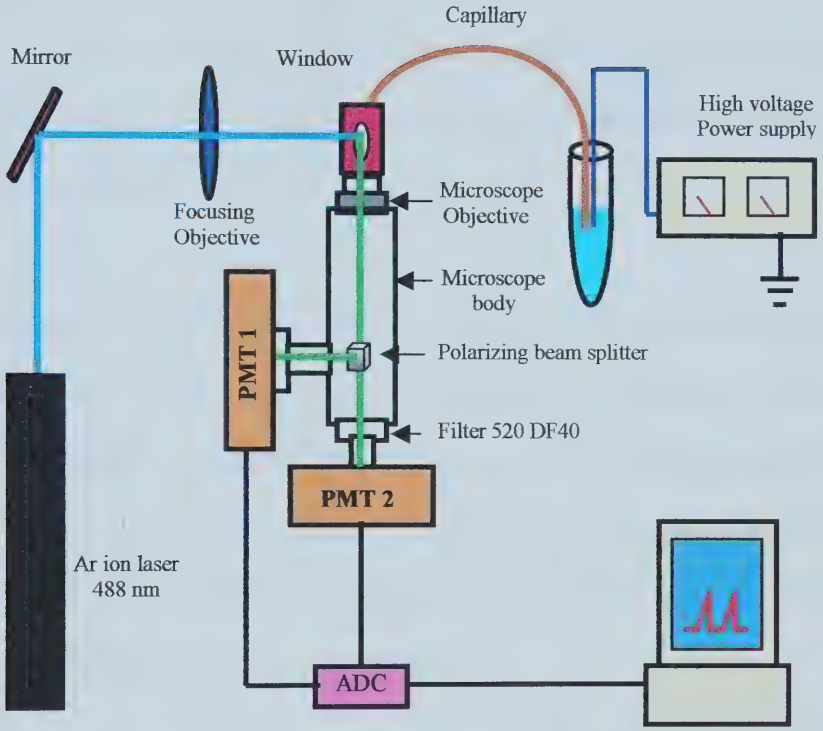

Figure 2.1 The schematic diagram of the CE/LIFP instrument

Fluorescence was collected with a 60× microscope objective lens (0.7 NA, Universe Kogaku, Oyster Bay, NY, USA), filtered through a narrow 515 nm band-pass filter (515DF20, Newport), and confined by a 2 mm pinhole. The fluorescence was split with a polarizing beam splitter (Melles Griot, Nepean, ON, Canada) to two photo multiplier tubes (PMT, R1477, Hamamatsu Photonics, Japan) to measure horizontally- and vertically-polarized light. A Power Macintosh computer controlled the high voltage and the acquisition of data with the application software written in LabView (National Instruments, Austin, TX, USA).

Fluorescein and BODIPY-FL were used when aligning the instrument to ensure that the maximum fluorescence signals were collected by both PMTs. An uncoated fused silica capillary was employed for CE separation. Although there is peak broadening due to protein absorption, conditioning the capillary with 20 mM NaOH regularly after each run is desirable and was performed to reduce the possibility of absorbed protein binding to the DNA aptamer.

Samples were electrokinetically injected into the capillary at 15 kV for 5 s, and the separation was carried out at 20 kV. 1× Tris-glycine (25 mM Tris, 192 mM glycine, pH 8.3) was used as running buffer. The capillary was conditioned after every injection with 20 mM NaOH at 10 kV for 10 min, followed by the running buffer at 20 kV for 10 min.

2.3 Results and Discussion

The aptamers are negatively charged under the CE separation conditions (pH 8-9). The isoelectric point of HIV-1 RT is around pH 8; its negative charge will be lowest in the running buffer (pH 8.3) [20]. When binding with highly negatively-charged aptamers, the complex will have a very different size-to-charge ratio than that of the aptamers. Therefore, the complex can be separated from the unbound aptamer by CE due to the differences in their electrophoretic mobilities. The migration times of the complexes are shorter than those of the DNA aptamers. The molecular weight of HIV-1 RT is 117 kDa, much larger than that of the DNA aptamers, which are around 25 kDa (RT1t49 is 15 kDa). The different stoichiometries of protein and aptamer can be separated because of the different size-to-charge ratios.

Interactions between proteins and the inner capillary wall can degrade the resolution and lead to adhesion of some of the proteins to the negatively-charged silanols on the capillary wall. That may be a reason why protein complexes of different stoichiometries are not easily resolved by free zone CE using uncoated fused silica capillary. Because the concentration of the protein used in this work was relatively low, uncoated capillaries were used to separate complexes and aptamers, and adsorbed proteins were removed by conditioning with NaOH after each run. The only problem is the band broadening of the complex peaks. The different stoichiometries may not have been well resolved from each other, but they were separated from aptamers very well.

2.3.1 Interaction of HIV-1 RT Protein with Aptamers RT12 and RT26

2.3.1.1 Binding of Aptamers with Varying Concentrations of HIV-1 RT

This study focuses on binding stoichiometry and demonstrates HIV-1 RT binding with a range of aptamers. RT12 is the aptamer most extensively studied here, and is shown to bind to HIV-1 RT in a similar manner as aptamer RT26. From Figure 2.2, two stoichiometries were formed by the increase of HIV-1 RT from 10 to 100 nM when the concentration of aptamer RT12 is maintained at a constant 32 nM in the mixture. RT26 also formed two stoichiometries with HIV-1 RT, depending on the molar ratio.

Figure 2.2 demonstrates a series of electropherograms from CE/LIF with aptamer RT12 concentration kept at 32 nM. Apparently, the HIV-1 RT can bind to more than a single aptamer; this additional binding occurs at lower protein concentration. The sharp peak of the aptamer has a migration time of ~3.6 min in the absence of HIV-1 RT, due to its negative effective charge, compared to the lower migration times (2.4-2.8 min) of the complexes formed in the mixtures. Affinity complex 1:2 clearly forms upon addition of a small amount of the HIV-1 RT, and has a migration time of ~2.8 min. Two complexes formed when the HIV-1 RT concentration was over 20 nM, resulting in a doublet peak or a peak with a shoulder. The peak corresponding to 1:1 stoichiometry has a migration time of ~2.4 min. The peak area of the second complex (stoichiometry 1:2) increases to its maximum when the HIV-1 RT is 35 nM, and then decreases as the HIV-1 RT concentration increases. The two complexes coexist until the HIV-1 RT concentration increases to ~80 nM. The peak area of the 1:1 complex increases to its maximum, while the 1:2 complex decreases. Quantitation of HIV-1 RT will be discussed in Chapter 5. The free aptamer and 1:2

complex peaks disappear completely when the HIV-1 RT concentration is greater than 80 nM. Only a single Gaussian peak represents the 1:1 stoichiometry, with a migration time of ~ 2.4 min. In these mixtures, when two complexes form between aptamer RT12 and HIV-1 RT, two stoichiometries were separated from the free aptamer, as follows:

$$\textbf{HIV-1 RT + RT12} = \underset{\textbf{(1:1 complex)}}{\textbf{HIV-1 RT (RT12)}} + \underset{\textbf{(1:2 complex)}}{\textbf{HIV-1 RT (RT12)}_2} \qquad (2\text{-}1)$$

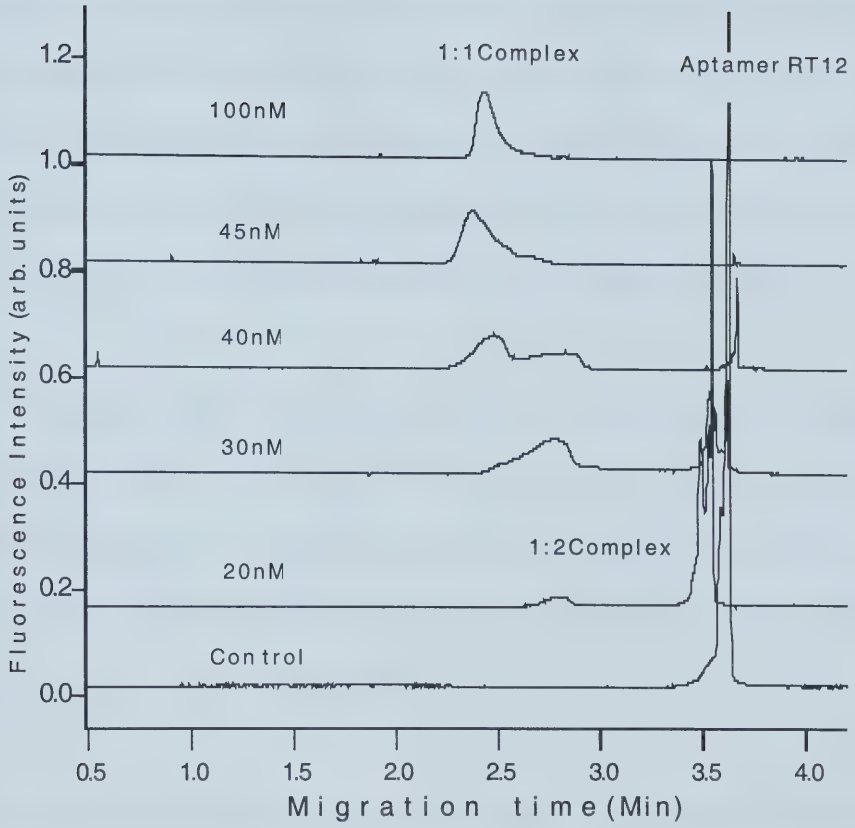

Figure 2.2 Electropherograms obtained from the analysis of incubation mixtures containing a fixed concentration of RT12 (32 nM) and varying concentration of HIV-1 RT. The bottom electropherogram contained only RT12 (32 nM). The capillary length is 40 cm. Samples were injected at 15 kV for 5 s. Separation was carried out at 20 kV. The running buffer is 1× Tris-glycine (25 mM Tris and 198 mM glycine, pH 8.3).

The migration time of aptamer RT12 is the longest (3.6 min) because it has the highest negative charge-to-size ratio among the three fluorescent species. The 1:1 complex between the protein and the aptamer has the lowest negative charge-to-size ratio, and therefore migrated out the fastest (2.4 min). The 1:2 complex between one protein and two aptamers has a charge-to-size ratio in-between the 1:1 complex and the unbound aptamer. Therefore its migration time is between the two (~ 2.8 min). Another aptamer, RT26, also forms two stoichiometries with HIV-1 RT depending on the molar ratio of the two components. These complexes have similar migration times to those of the RT12 complexes. The formation equation (2-1) also applies to RT26.

The unbound HIV-1 RT could not be observed from the electropherogram because no fluorophore was attached to it. The two complexes could not be well separated by capillary electrophoresis, because their electrophoretic mobilities were close, and because of the band-broadening of the peaks probably caused by adsorption and desorption of the protein to the capillary wall.

2.3.1.2 Binding of HIV-1 RT Protein with Varying Concentrations of Aptamer RT12

Another approach was to add aptamer RT12 to a constant HIV-1 RT concentration (50 nM). The conclusion that the two complexes formed were dependent on the relative molar ratio can be affirmed (Figure 2.3). By increasing the concentration of RT12 from 2.67 nM to 128.0 nM, it is seen that 1:1 stoichiometry dominates at lower RT12 concentrations when the protein is in much excess, while the

1:2 complex and the free aptamer coexist with the 1:1 complex at higher RT12 concentrations, when the aptamer is in large excess. With HIV-1 RT in excess, only the 1:1 complex peak can be observed. The peak area of the 1:1 complex is at its maximum at ~28 nM aptamer. The peaks of the 1:2 complex and the unbound aptamer increase with the increase of aptamer concentration. The peak area of the 1:2 complex is saturated when all HIV-1 RT is consumed to form the 1:2 complex. Both Figures 2.2 and 2.3 show that the formation of the two complexes depends on the molar ratio of HIV-1 RT and the aptamer from both titration curves. When HIV-1 RT is in excess, the 1:1 stoichiometry dominates; however, when RT12 is in excess, 1:2 stoichiometry is more favorable and always coexists with the unbound aptamer peak.

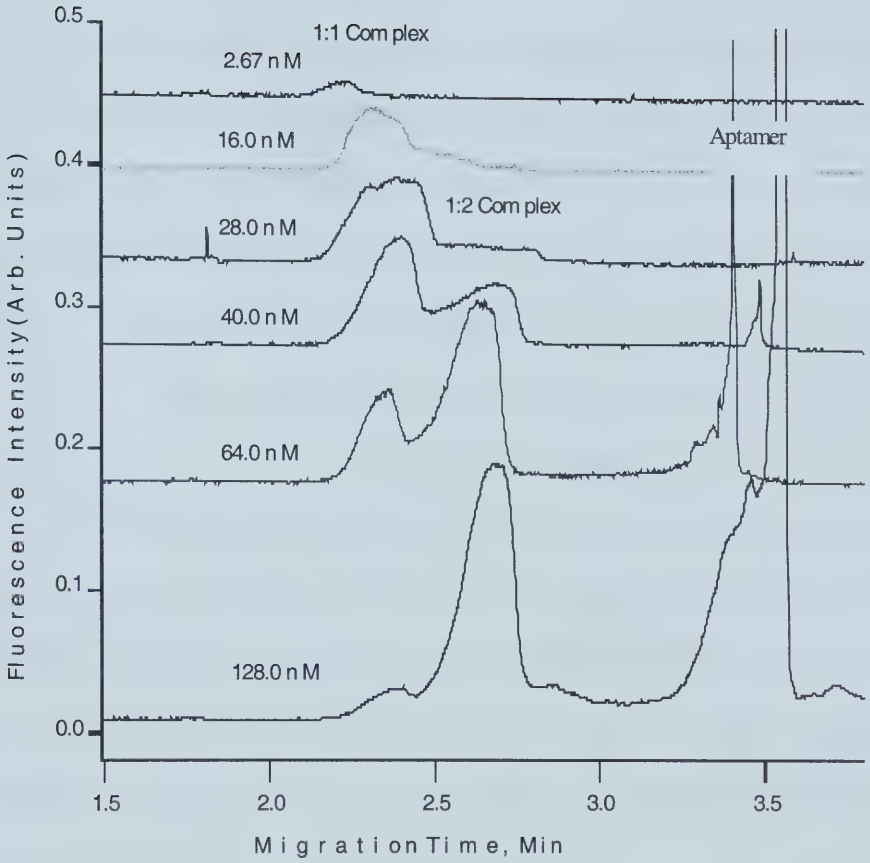

Figure 2.3 Electropherograms obtained from the analysis of incubation mixtures containing a fixed concentration of HIV-1 RT (50 nM) and varying concentration of RT12. The same CE/LIF conditions as in Figure 2.2 were used.

2.3.2 Interaction of HIV-1 RT Protein with Aptamer RT1t49

Aptamer RT1t49 was introduced in the binding study with HIV-1 RT because of its shorter length than RT12 and RT26, and its binding affinity, which is at the same level. The electropherograms from the titration of RT1t49 with varying concentration of HIV-1 RT are shown in Figure 2.4. Only one complex was observed, and there was no double peak or peak with a shoulder in the electropherogram. The migration time of this complex (2.2-2.6 min) is consistent with that of the 1:1 complex formed between the protein and aptamers RT12 (~2.4 min) and RT26 (~2.4 min). The formation of the complex of 1:1 stoichiometry could be described by:

$$\textbf{HIV-1 RT + RT1t49 = HIV-1 RT (RT1t49)} \qquad (2\text{-}2)$$

1:1 complex

Electropherograms from the analysis of incubation mixtures containing a constant HIV-1 RT concentration (50 nM) while the concentration of aptamer RT1t49 (4-76 nM) is varied are illustrated in Figure 2.5. A complex of one stoichiometry was observed, and it was separated from the aptamer by CE/LIF. The similar migration time to that of the 1:1 stoichiometry suggests that this is a 1:1 complex between the protein and aptamer RT1t49.

Aptamer RT1t49 is known to bind with the polymerase site but not the RNase H site of HIV-1 RT protein [8]. The observation of only 1:1 complex (Figures 2.4 and 2.5) provides supporting evidence. The results suggest that the two binding sites responsible for the formation of 1:1 and 1:2 complexes are not identical and may bind to different regions of the aptamer.

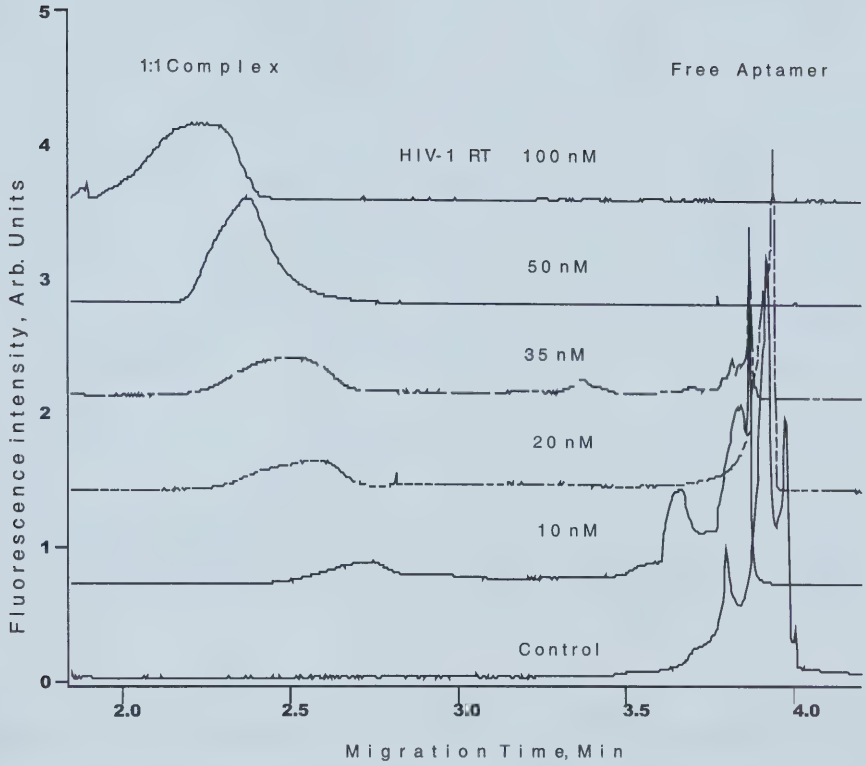

Figure 2.4 Electropherograms obtained from the CE/LIF analysis of samples containing a fixed concentration of RT1t49 (32 nM) and varying concentration of HIV-1 RT. The bottom electropherogram contained RT1t49 (32 nM) only. The aptamer peak corresponds to RT1t49; the peak complex corresponds to 1:1 stoichiometry of RT1t49 and HIV-1 RT. The same CE/LIF conditions as in Figure 2.2 were used.

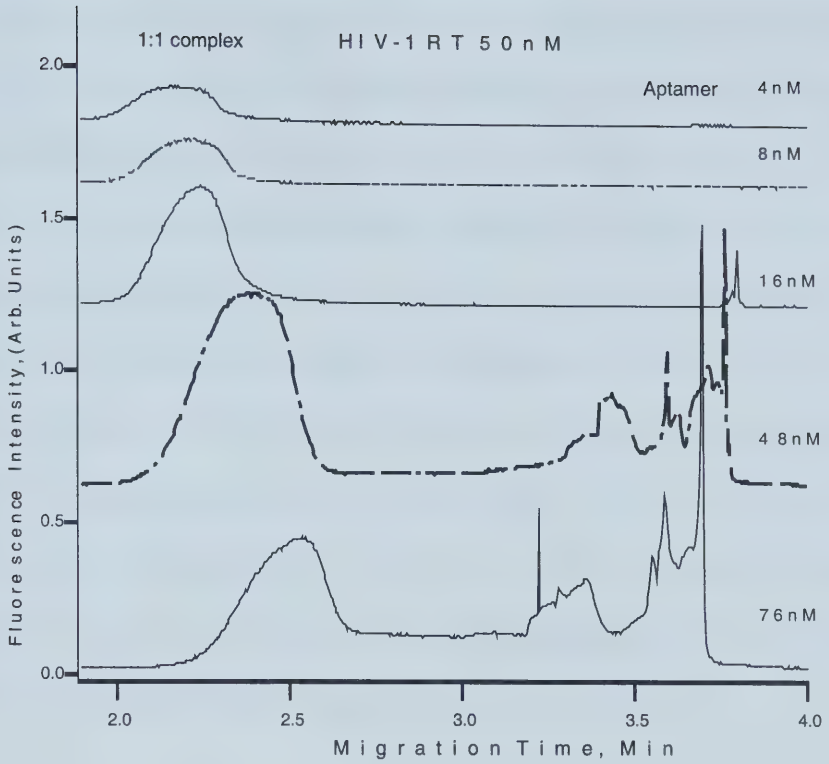

Figure 2.5 Electropherograms obtained from the CE/LIF analysis of samples containing a fixed concentration of HIV-1 RT (50 nM) and varying concentration of RT1t49. The aptamer peak corresponds to free RT1t49; the peak complex corresponds to the 1:1 complex of RT1t49 and HIV-1 RT. The same CE/LIF conditions as in Figure 2.2 were used.

2.3.3 Interaction of HIV-1 RT Protein with Aptamer ODN93

To gain further information about the binding of HIV-1 RT protein with different forms (and regions) of aptamers, the interaction of aptamer ODN93 with HIV-1 RT was studied. This aptamer was initially developed to inhibit the RNase H activity, but it was found that it inhibits the polymerase activity as well. Aptamers RT12 and RT26 were developed to inhibit the polymerase activity of HIV-1 RT. It was not known whether they were recognized by the RNase H site. Our results show that these aptamers can probably bind with both sites of the protein, as seen by the formation of both 1:1 and 1:2 complexes. The interaction of ODN93 with HIV-1 RT protein is similar to that of RT12 and RT26, shown in Figure 2.6. There is an impurity in ODN93, making the aptamer peak broader than those of RT12 and RT26, and also possibly leading to the double peak of complexes emerging as a single broad peak. Although the two complexes are not well resolved, the presence of both 1:1 and 1:2 complexes are apparent from the complex peaks with shoulders.

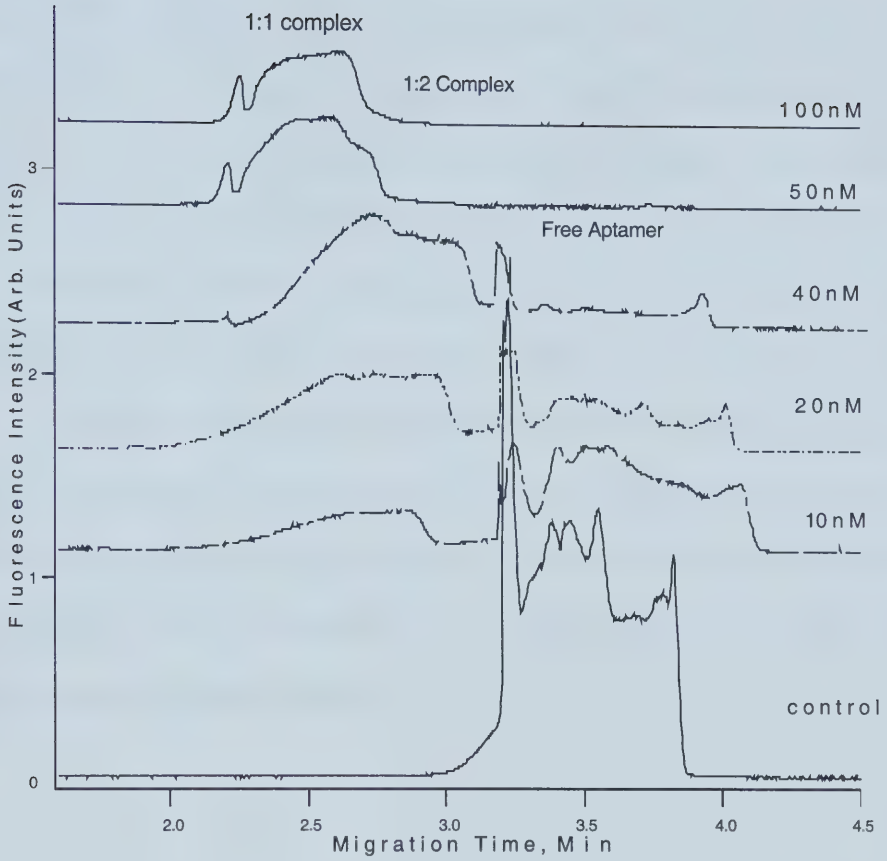

Figure 2.6 Electropherograms obtained from the CE/LIF analysis of samples containing a fixed concentration of ODN93 (32 nM) and varying concentration of HIV-1 RT. The bottom electropherogram contained ODN93 (32 nM) only. The same CE/LIF conditions as in Figure 2.2 were used.

2.4 Conclusion

A CE/LIF technique was developed to study the interactions of HIV-1 RT protein with four aptamers *in vitro*. The unbound fluorescently-labeled aptamers were separated from the protein-aptamer complexes by CE, and both the unbound and protein-bound aptamers were detected by LIF. The CE/LIF analysis revealed the 1:1 and 1:2 complexes between the HIV-1 RT protein and each of the aptamers RT12, RT26, and ODN93, suggesting that these aptamers can bind at both the polymerase site and the RNase H site of the HIV-1 RT protein. A shorter aptamer, RT1t49, was able to form a 1:1 complex with the HIV-1 RT protein, probably because it was recognized by the polymerase site only. Additional study is required to support these findings and conclusions. More information can be obtained by using fluorescence polarization to study the nature of the interactions between the aptamers and HIV-1 RT protein; this will be discussed in the next chapter.

2.5 Reference

1. Skalka, A.M.; Goff, S.P.(ed.) *Reverse Transcriptase* Cold Spring Harbor Laboratory Press, New York, **1993**
2. Jonckheere, H; Snne, J.; De Clercq, E. H. *Med. Res. Rev.* **2000**, 20, 129-154
   The HIV-1 RT process as Target for RT inhibitors
3. Turner, B.G.; Summers, M.F. *J. Mol. Biol.* **1999**, 285, 1-32
   Structural Biology of HIV
4. Jonckheere, H.; De Vreese, K.; et al *J. Virol. Methods* **1996**, 61, 113-125
   Functionality of the subunits of the reverse transcriptase of the human immunodeficiency virus type I
5. Jacobo-Molina, A.; Ding, J.; et al *PNAS USA* **1993**, 90, 6320-6324
   Crystal Structure of HIV-1 RT complexed with ds-DNA at 3.0 A resolution shows bent DNA
6. Gao, H.Q.; Sarafianos, S.G.; Arnold, E.; Hughes, S.H. *J. Mol. Biol.* **1999**, 294, 1097–1113
   Similarities and differences in the RNase H activities of HIV-1 RT and Moloney murine leukemia virus RT
7. Schatz, O.; Mous, J.; Le Grice, S.F.J. *EMBO J.* **1990**, 9, 1171–1176
   HIV-1 RT-associated ribonuclease H displays both endonuclease and 3'→5' exonuclease activity
8. Schneider, D. J.; Feignon, J.; Hostomsky, Z.; Gold, L. *Biochemistry* **1995**, 34, 9599-9610
   High-affinity ssDNA inhibitors of the reverse transcriptase of type 1 human immunodeficiency virus
9. Andreola, M. L.; Pileur, F.; Calmels, C.; Ventura, M.; Tarrago-Litvak, L.; Toulme, J. J.; Litvak, S. *Biochemistry* **2001**, 40, 10087-10094
   DNA Aptamers Selected against the HIV-1 RNase H Display in Vitro Antiviral Activity
10. Pavski, V.; Le, X. C. *Anal. Chem.* **2001**, 73, 6070-6076
    Detection of Human Immunodeficiency Virus Type 1 Reverse Transcriptase Using Aptamers as Probes in Affinity Capillary Electrophoresis
11. Rippel, G.; Gorstjen, H.; Billiet, H.A.H.; Frank, J. *Electrophoresis* **1997**, 18, 2175-2183

Affinity capillary electrophoresis

12. Chu, Y.-H.; Avila, L.Z.; et al *Acc. Chem. Res.* **1995**, 28, 461-468
Affinity capillary electrophoresis

13. Galbusera, C.; Chen, D.Y. *Curr. Opin. Biotech.* **2003**, 14, 126-130
Molecular interaction in capillary electrophoresis Studied by Capillary Electrophoresis and Laser-Induced Fluorescence

14. Cassiday, L. A.; Lebruska, L. L.; et al *Anal. Biochem.* **2002**, 306, 290-297
Binding Stoichiometry of an RNA aptamer and its Transcriptase Factor Target

15. Rosu, F.; Gabelica, V.; Houssier, C.; Colson, P.; Pauw, E. D. *Rapid Commun. Mass Spactrom.* **2002**, 16, 1729-1736
Triplex and quadruplex DNA structures studied bt electrospray mass spectrometry

16. Cowan, J. A.; Ohyama, Tsuyoshi; Wang, D.; Natarajan, K. *Nucleic Acids Res.* **2000**, 28, 2935-2942
Recognition of a cognate RNA aptamer by neomycin B: quantitative evaluation of hydrogen bonding and electrostatic interactions

17 Wan, Q.H.; Le, X.C. *J. Chromatogr. B* **1999**, 734, 31-38
Capillary electrophoresis immunoassays for digoxin and gentamicin with laser-induced fluorescence polarization detection

18. Wan, Q.H.; Le, X.C. *Anal. Chem.* **2000**, 72, 5583-5589
Studies of protein-DNA interactions by capillary electrophoresis laser-induced fluorescence polarization

19. Le, X.C.; Wan, Q.H.; Lam, M.T. *Electrophoresis* **2002**, 23, 903-908
Fluorescence polarization detection for affinity capillary electrophoresis

20. Bhikhabhai, R.; et al *J. Chromatogr.* **1992**, 604, 157-170
Purification, characterization and crystallization of recombinant HIV-1 RT

Chapter 3 Fluorescence Polarization Study of Aptamers Binding with HIV-1 RT

3.1 Introduction

3.1.1 Fluorescence Polarization Combined with CE/LIF

Fluorescence polarization (FP) is an intrinsic property of molecules. It provides evidence of complex formation with large biomolecules [1-3]. It has been employed in applications such as competitive immunoassay detection of antibody-antigen binding [4], the detection of DNA hybridization [5], DNA-protein binding [6], protein-ligand binding, and enzyme assays [7]. When combined with separation techniques such as affinity capillary electrophoresis (ACE), FP measurement of individual complexes provides additional information on binding interactions. An ACE/LIFP method has been demonstrated in the study of ligand-protein and protein-DNA binding by simultaneous measurement of electrophoretic mobility and FP [11-15].

In this research, the FP technique is combined with ACE to examine the different stoichiometries of complexes formed between HIV-1 RT and the aptamers. This combination is very helpful for the identification of complexes formed between small probes and large biomolecules. It provides information not only about the mass-to-charge ratio of all components, but also about the size of the complexes. The assignment of peaks of different stoichiometries may be difficult in ACE due to small shifts in migration times, or to poor resolution of complexes formed between the protein and the other binding partners. During CE separation, the FP values of different

peaks can be determined simultaneously, allowing more structural information to be revealed. Another advantage is the differentiation between different stoichiometries.

Initially, FP was used to monitor the binding stoichiometries. The discovery that the FP of the complexes of 1:2 stoichiometry is smaller than that of the complexes of 1:1 stoichiometry between RT12 or RT26 and HIV-1 RT was surprising. To understand the possible reason for this, RT1t49 and ODN93 were introduced to bind with the same protein, so that the FP of the complexes could be compared.

3.1.2 Fluorescent Labeling

5-FAM, 5-Carboxyfluorescein, a derivative of fluorescein, was used in this work. The structure of this dye can be found in Figure 3.1. It was covalently attached to the aptamers on the 5' end (Figure 3.2), obtained from University Core DNA Services (University of Calgary, Calgary, AB, Canada). This dye is efficiently excited by the 488 nm spectral line of the Ar ion laser, and emits at 520 nm. The absorption and emission spectra of 5-FAM in pH 9 buffer are illustrated in Figure 3.3. The absorption and emission spectra of 5-FAM overlap.

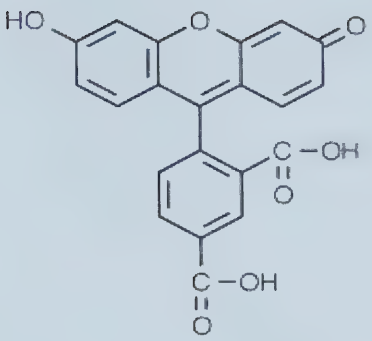

Figure 3.1 Structure of 5-Carboxyfluorescein (5-FAM)

Molecular Formula: $C_{21}H_{12}O_7$

Molecular Weight: 376.32

Name: Spiro (isobenzofuran-1(3H), 9'-(9H) xanthene)
-5-carboxylic acid, 3', 6'-dihydroxy-3-oxo

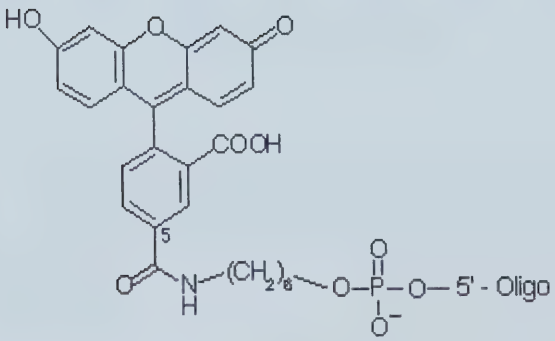

Figure 3.2 Structure of 5-FAM, after attachment to an oligonucleotide

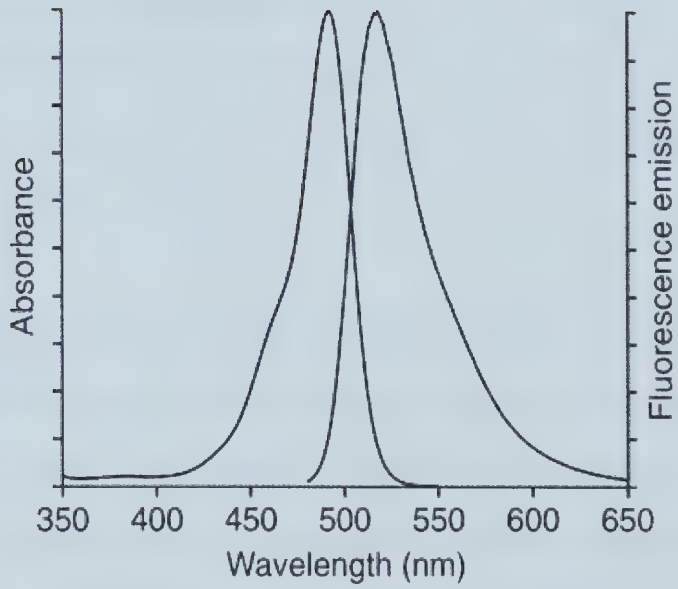

Figure 3.3 Absorption and fluorescence emission spectra of 5-carboxyfluorescein (5-FAM), overlapping. The buffer was 0.1 M borate, pH 9.0.

3.2 Experimental

3.2.1 CE-LIFP Analysis

The home-built CE coupled with the LIFP instrument has been described previously in Chapter 2. Untreated fused silica capillaries (20 μm i.d., 150 μm o.d.) were used for separation. The typical length of the capillaries was 40 cm, (later cut to 25 cm for faster separation), and the applied electric field was 500 V/cm (800 V/cm for 25 cm capillary). Unless stated otherwise, 1 × Tris-glycine (25 mM Tris, 198 mM glycine, pH 8.3) was used as running buffer. The separation was carried out at ambient temperature. Other experimental procedures were the same as described in Chapter 2.

Optimal performance of the LIFP detector was achieved by aligning the detection window that held the capillary with respect to the incident laser light and the fluorescence detection optics. This was carried by balancing the signals collected by the two PMTs when fluorescein or BODIPY-FL was allowed to flow through the capillary. The voltage of the horizontal PMT was set at 1000 V, while the voltage of the vertical PMT was adjusted by injecting fluorescent dye, when equal signals came from two PMTs deprived of background. The degree of FP is defined by [1-2]:

$$P = (I_V - I_H) / (I_V + I_H) \qquad (3\text{-}1)$$

where I_V and I_H are the fluorescence intensities of vertically- and horizontally-polarized components.

There is a possibility that the signals collected from the two PMTs are not equal. The voltage of the PMTs can be adjusted until the signals from both of them are identical when monitoring the fluorescence of BODYPY-FL dye or fluorescein. It has been assumed that the polarization and anisotropy of the BODYPY-FL dye or fluorescein are negligible, due to the relatively small size of the dyes.

3.2.2 Reagents and Stock Solutions

The reagents and stock solutions used are the same as described in 2.2.1. RT26 and ODN93 are 81-mers, RT12 is an 84-mer and RT1t49 is a 49-mer. Their molecular weights are summarized in Table 3.1 (not including the fluorescent dye).

Table 3.1 MW of Aptamers and HIV-1 RT

Name	Length	MW	MW of 1:1 Complex	MW of 1:2 Complex
RT12	84-mer	27,200	145,000	172,200
RT26	81-mer	26,300	144,100	170,400
RT1t49	49-mer	15,900	133,700	N/A
ODN93	81-mer	26,600	144,400	171,000
HIV-1 RT	Heterodimer	117,800	N/A	N/A

3.3 Results and Discussion

3.3.1 Fluorescence Polarization of the Complexes between aptamer RT12 and HIV-1 RT

Figure 3.4 shows electropherograms from the analysis of aptamer RT12. Fluorescence intensities from two polarization planes, horizontal (I_H) and vertical (I_V), were simultaneously detected. The concentration of aptamer RT12 was kept at 32 nM. This was the concentration used in most of the experiments described in this chapter. Results of FP over the entire separation window were obtained and plotted along with the electropherogram. Usually only the FP of the peak is reported. It can be seen that FP values were around 0.015 to 0.025 for the aptamer, which had a migration time of 3.45 min.

Figure 3.5 shows the presence of the unbound aptamer and the aptamer-protein complexes. The fluorescence intensity from the two polarization planes (I_V and I_H), as well as the FP values, was measured. Two complexes migrated at 2.40 and 2.70 min, and were well separated from the unbound aptamer RT12 (3.50 min). The migration time of the unbound aptamer was consistent with that of the aptamer in the absence of protein. The measurement of FP shows that the complex of 1:1 stoichiometry has the highest FP value, 0.10, and the aptamer has the lowest, 0.02. The complex of 1:2 stoichiometry has an FP value of 0.06. There is an overlap of the 1:1 and the 1:2 stoichiometries; the FP decreases gradually from 0.10 to 0.06, and then to 0.02. Although the two complexes may not be well separated, qualitative information can be obtained to determine the two individual complexes from their migration times and FP values.

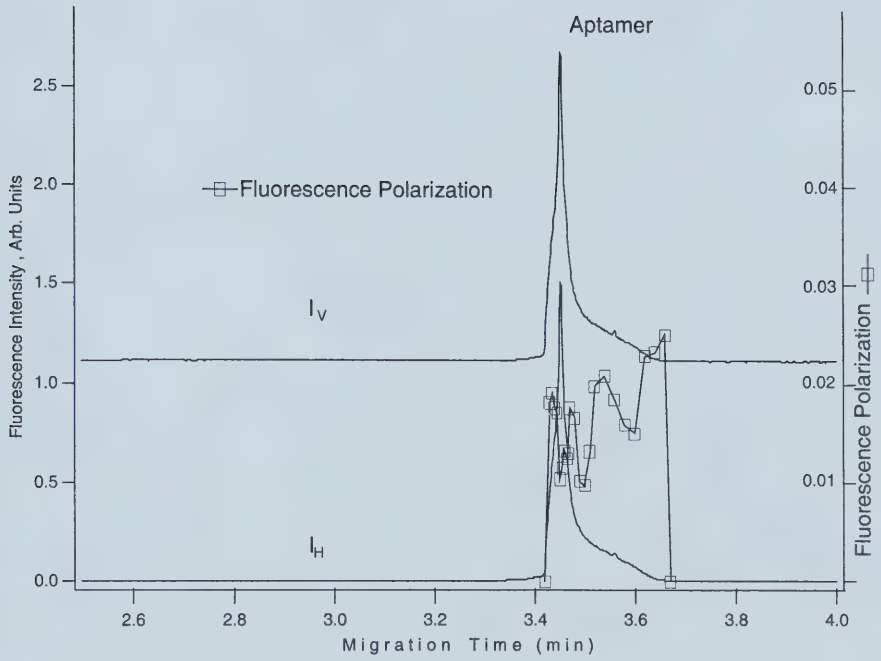

Figure 3.4 Electropherograms showing the vertically- and horizontally-polarized fluorescence (the left Y-axis) and FP (the right Y-axis) of aptamer RT12. I_V and I_H correspond to the vertical and horizontal fluorescence intensities, respectively. The RT12 concentration was 32 nM. I_v was offset in the Y-axis for clarity. Fused silica capillaries (40 cm long, 20 μm i.d., 150 μm od.) were used. The running buffer was 1 × Tris-glycine (25mM Tris, 192 mM glycine, pH 8.3). The separation voltage was 20 kV.

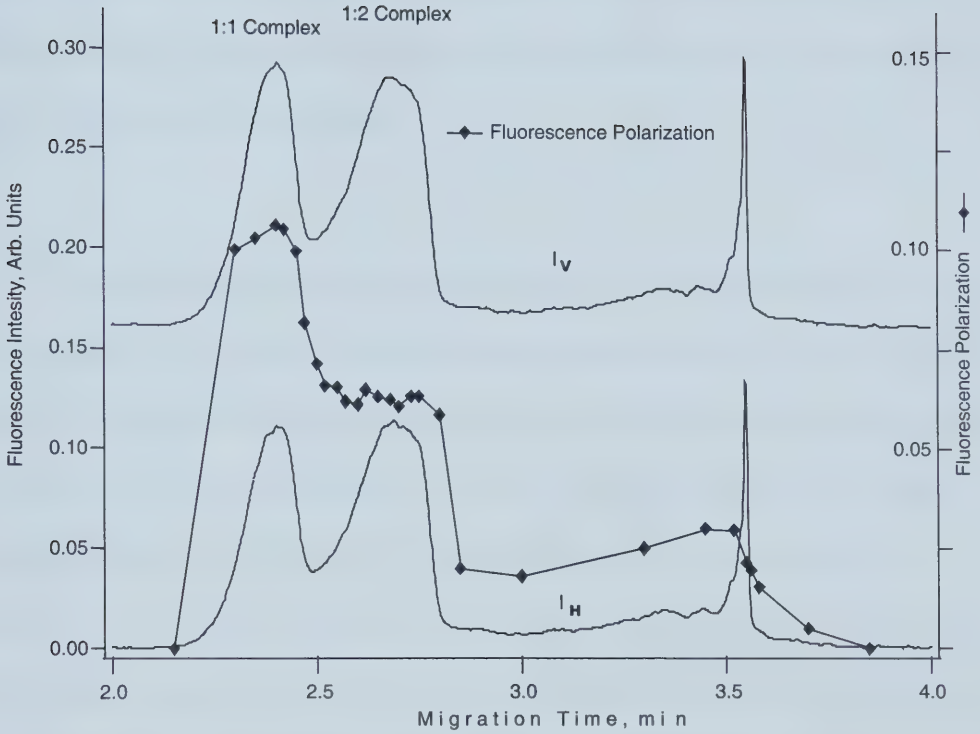

Figure 3.5 Electropherograms showing the vertically- (I_V) and horizontally- (I_H) polarized fluorescence. The FP values were also plotted, showing substantial polarization where the complexes appeared. RT12 was 32 nM, and HIV-1 RT was 35 nM. Two stoichiometries were observed as a double peak. I_V was offset in the Y-axis for clarity. The same CE/LIFP conditions as in Figure 3.4 were used.

Figure 3.6 shows electropherograms of the 1:1 stoichiometric complex between the excess protein and the limiting amount of aptamer RT12. The FP value of the complex was approximately 0.11 to 0.13. With HIV-1 RT concentration much higher than that of RT12, no peaks of the complex of the 1:2 stoichiometry and the unbound aptamer were observed. The predominant complex was of 1:1 stoichiometry between the aptamer and the protein.

In contrast, when the aptamer concentration was in excess of the HIV-1 RT concentration, the complex of 1:2 stoichiometry was predominant (Figure 3.7). The FP value of the complex was approximately 0.05 to 0.06. The CE separation did not show the presence of the 1:1 stoichiometric complex. However, a small part of the peak at migration time of 2.4 min had an FP value higher than 0.06, suggesting that the complex of 1:1 stoichiometry might be present. The FP values in the electropherogram between the complex of 1:2 stoichiometry and the unbound aptamer were higher than baseline, suggesting dissociation of the complex. Thus, FP measurements provide additional information that is not revealed by CE.

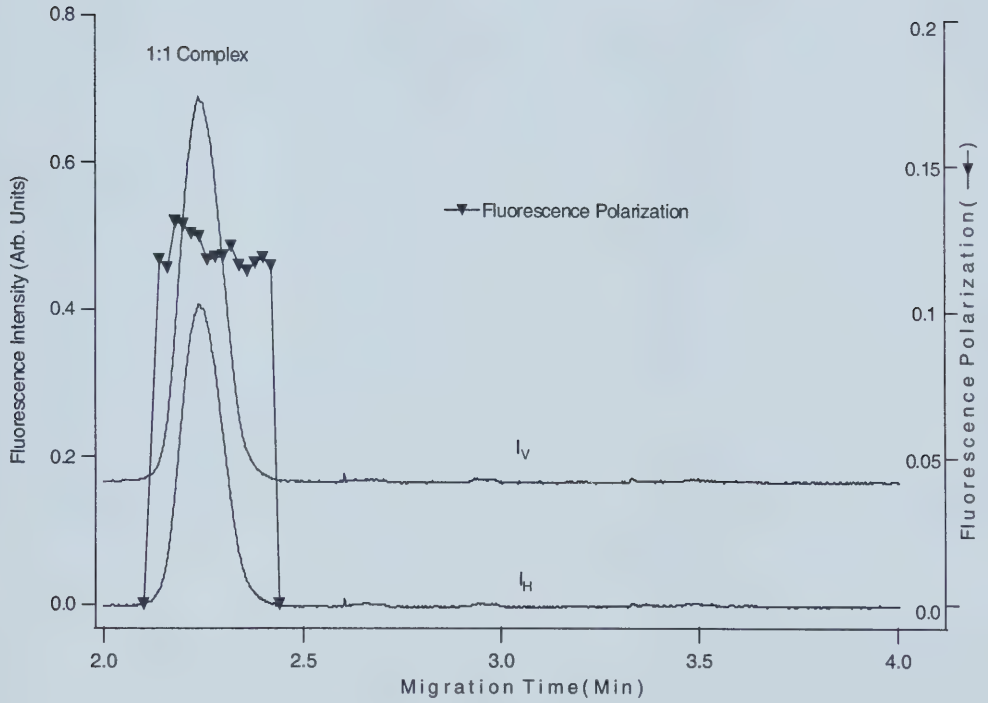

Figure 3.6 Electropherograms showing vertically- and horizontally- polarized fluorescence and FP of the 1:1 complex. I_V and I_H correspond to vertical and horizontal fluorescence intensities, respectively. The concentration of RT12 was 32 nM, and that of HIV-1 RT was100 nM. The limiting amount of aptamer (RT12) favored the formation of the 1:1 complex. No peaks of the complex of 1:2 stoichiometry and unbound aptamer RT12 were observed. I_V was offset in the Y-axis for clarity. The same CE/LIFP conditions as in Figure 3.4 were used.

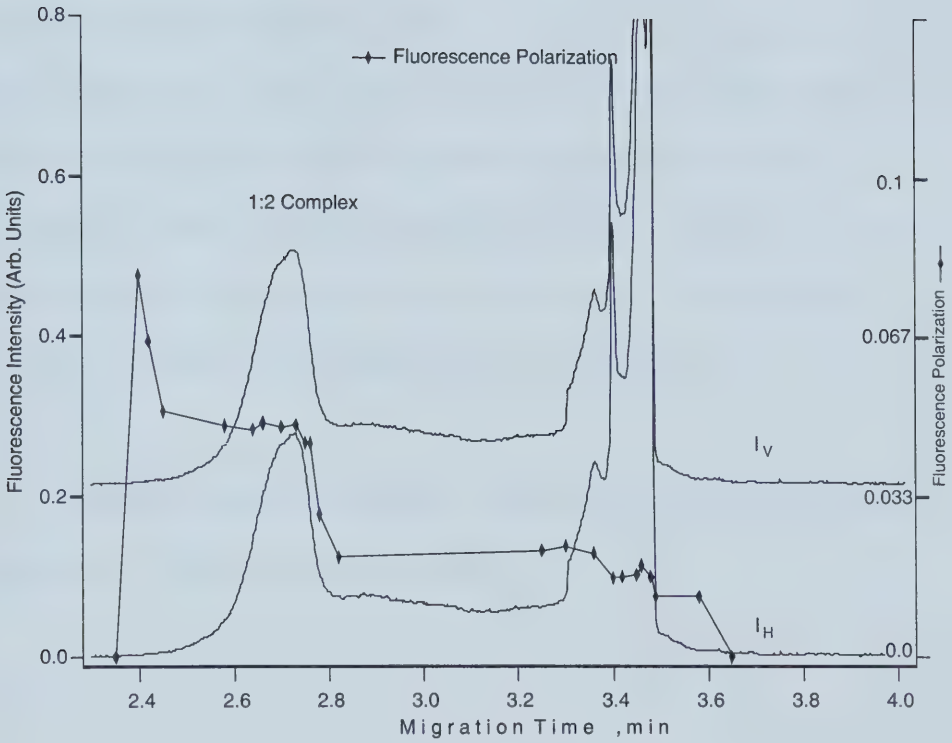

Figure 3.7 Electropherograms showing vertically- and horizontally-polarized fluorescence (the left Y-axis) and FP (the right Y-axis) of aptamer RT12 and its complexes with HIV-1 RT. I_V and I_H correspond to vertical and horizontal fluorescence intensities, respectively. The concentration of RT12 was 32 nM, and that of HIV-1 RT was 20 nM. The presence of excess amount of aptamer (RT12) over the protein (HIV-1 RT) favored the formation of the 1:2 complex that consists of one protein and two aptamers. I_V was offset in the Y-axis for clarity. The same CE/LIFP conditions as in Figure 3.4 were used.

A summary of the FP measurements of the aptamer-protein complexes and the unbound aptamer is shown in Figure 3.8. The FP value is always highest for the complex of 1:1 stoichiometry. The complex of 1:2 stoichiometry has an FP value between that of the complex of 1:1 stoichiometry and that of the aptamer, while the aptamer has the lowest FP value. All species can be differentiated from the FP curve. From the polarization measurement at the peak of the electropherogram, the unbound aptamer in the absence of HIV-1 RT has an FP of 0.013 ± 0.002. Upon binding with HIV-1 RT, the FP values increase. The protein bound with one aptamer (1:1 stoichiometry) has the highest FP value of 0.127 ± 0.026. The protein bound with two aptamers (1:2 stoichiometry) has FP of 0.060 ± 0.011. These FP values are measured from the peaks of the complexes that are separated by CE.

Possible reasons for the lower FP values of the 1:2 complex compared to those of the 1:1 complex will be discussed later.

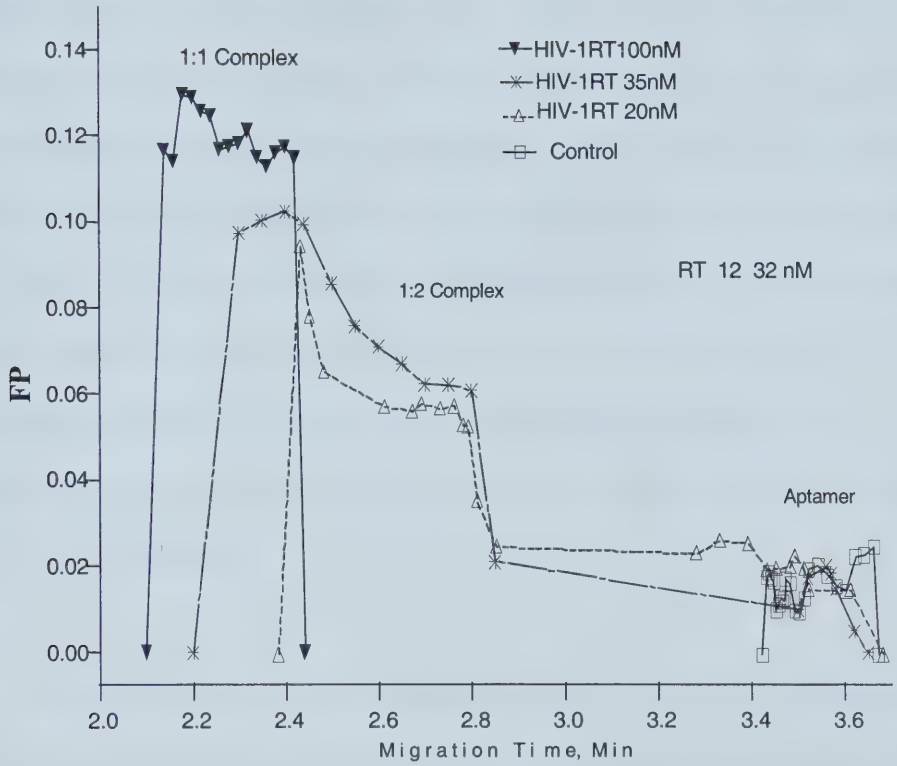

Figure 3.8 FP curve of complexes and the unbound aptamer RT12. The concentration of RT12 is kept constant at 32 nM, while the concentration of HIV-1 RT varies.

3.3.2 Fluorescence Polarization of the Complex between Aptamer RT1t49 and HIV-1 RT

In Chapter 2, results from the CE separation showed that only one complex was formed between the protein HIV-1 RT and the aptamer RT1t49. Formation of the 1:1 complex is further supported by the FP results, as shown in Figure 3.9. In this experiment, the capillary was cut shorter (25 cm) and consequently, the migration times for both the aptamer and the complex were shorter. The FP value of the complex was 0.125 ± 0.024, similar to the FP value of the 1:1 stoichiometric complex of RT12 and HIV-1 RT (0.127). The FP value of the free unbound aptamer was ~ 0.020, consistent with its smaller size. The FP values of the complex formed between varied concentrations of HIV-1 RT and the aptamer were also measured. They were consistently between 0.12 and 0.14, regardless whether aptamer RT1t49 or the protein HIV-1 RT was in excess.

These results suggest that the complex between HIV-1 RT protein and aptamer RT1t49 has 1:1 stoichiometry and that there is no indication of the 1:2 complex. These results are consistent with the literature reports that aptamer RT1t49 is recognized only at the polymerase site of the HIV-1 RT protein [16].

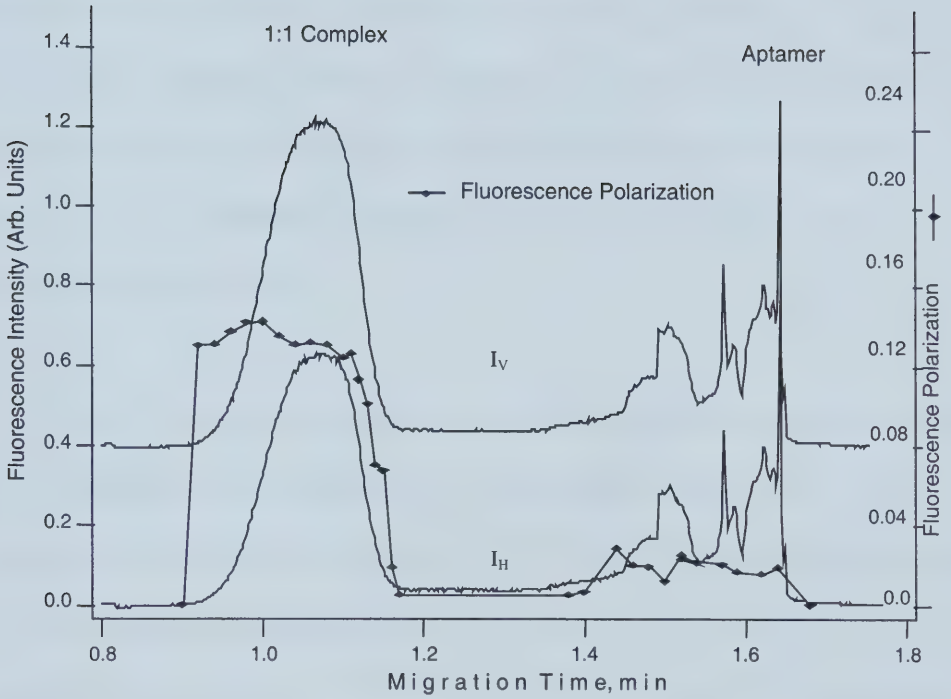

Figure 3.9 Electropherograms showing vertically- and horizontally-polarized fluorescence (the left Y-axis) and FP (the right Y-axis) of aptamer RT1t49 and its complex with the protein. I_V and I_H correspond to vertical and horizontal fluorescence intensities, respectively. The concentration of RT1t49 was 32 nM, and that of HIV-1 RT was 35 nM. I_V was offset in the Y-axis for clarity. Separation was carried out using a 25 cm capillary. Other conditions were the same as those shown in Figure 3.4.

3.3.3 Fluorescence Polarization of the Complexes between RT26 and ODN93 with HIV-1 RT

The CE results in Chapter 2 have shown that the three full-length aptamers, RT12, RT26, and ODN93, formed both 1:1 and 1:2 complexes with the protein HIV-1 RT, whereas the shorter aptamer, RT1t49, formed only a complex of 1:1 stoichiometry with the protein. The FP values of the complexes involving RT12 (Figure 3.8) and RT1t49 (Figure 3.9) provide additional supporting evidence. Thus, the application of FP measurements to differentiate the 1:1 complex from the 1:2 complex is further demonstrated for the complex between the protein HIV-1 RT and the other two aptamers, RT26 and ODN93.

Figure 3.10 shows the results from the analysis of a mixture solution containing 32 nM aptamer RT26 and 30 nM HIV-1 RT. Two complexes migrated at 1.1 and 1.3 min, and were separated from the unbound RT26 (1.7 min). It appears that the complex of 1:1 stoichiometry has a higher FP value (0.098) than the 1:2 complex (0.039). The unbound aptamer has the lowest FP value (0.020). The FP values of the complexes and the unbound aptamer RT26 follow the same trend as those of aptamer RT12 (Figure 3.5).

Figure 3.11 shows the FP values from the analysis of aptamer ODN93 and its complexes with HIV-1 RT. The 1:1 complex has a higher FP value (0.124) than the 1:2 complex (0.076). These results are consistent with those shown in Figure 3.8 where aptamer RT12 was used.

The FP values of the complex of 1:1 stoichiometry are very similar for all the four aptamers, while there is a difference between the FP values of the complex of 1:2 stoichiometry of RT12, RT26, and ODN93. Of the 1:2 stoichiometric complexes, RT26 has the lowest FP, 0.039 ± 0.005, RT12 has an FP value of 0.060 ± 0.011, and ODN93 has the highest, 0.076 ± 0.014. They are all lower than those of the 1:1 stoichiometries and higher than those of the aptamers.

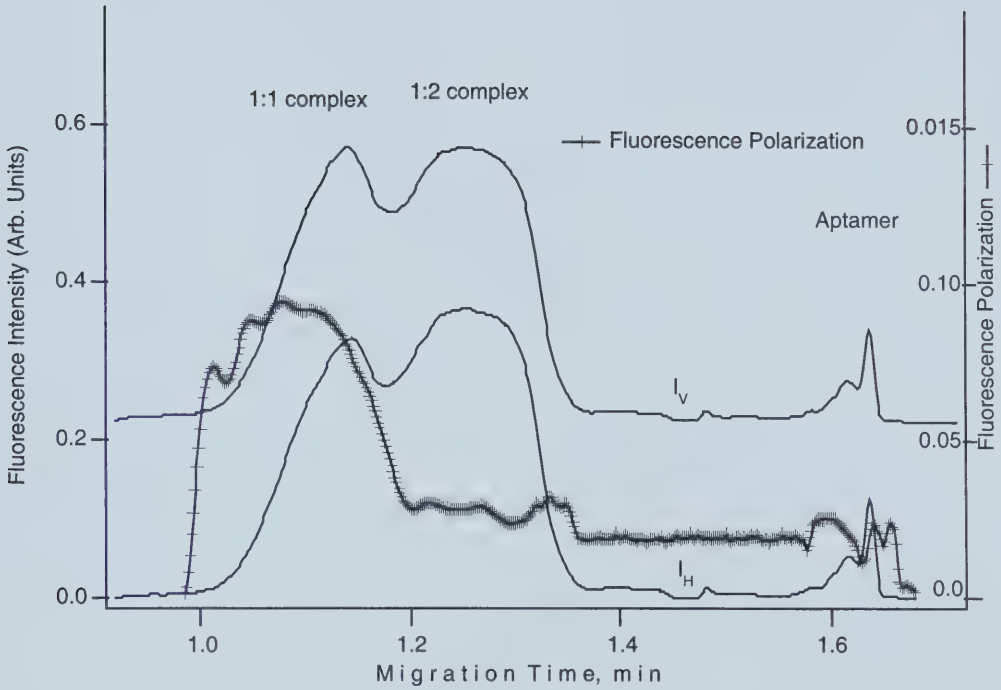

Figure 3.10 Electropherogram showing vertically- and horizontally-polarized fluorescence and FP of aptamer RT26 and its complexes with the protein HIV-1 RT. I_V and I_H correspond to vertical and horizontal fluorescence intensities, respectively. The concentration of RT26 was 32 nM, and that of HIV-1 RT was 30 nM. Two stoichiometries were observed as double peaks with different FP values. The I_v was offset in the Y-axis for clarity. Separation was carried out in a 25-cm capillary. Other conditions were the same as those shown in Figure 3.4.

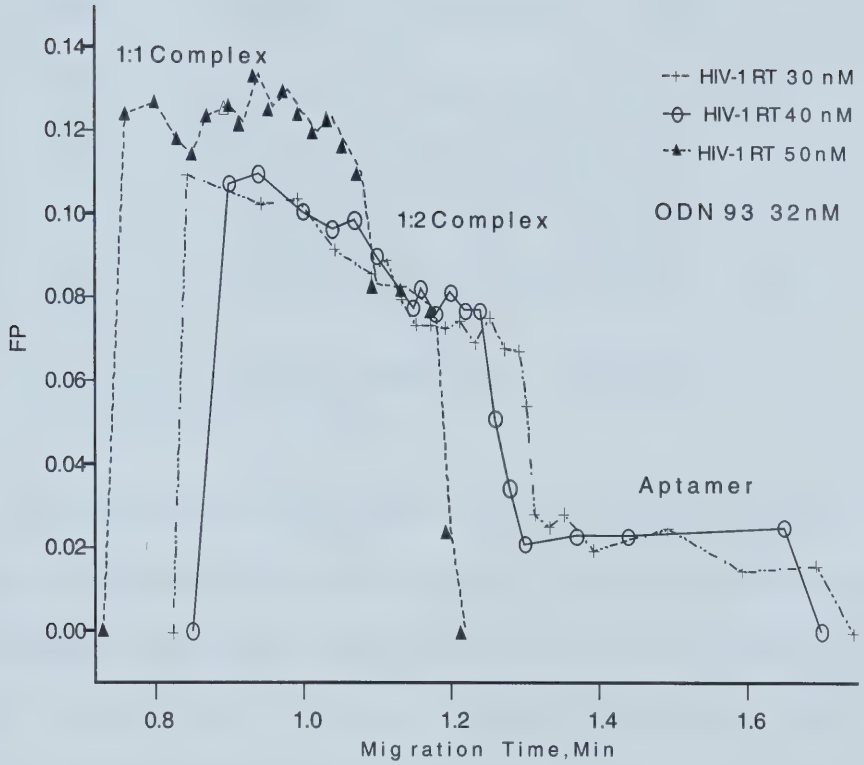

Figure 3.11 FP values of complexes between HIV-1 RT and aptamer ODN93, separated from the free aptamer ODN93. The concentration of ODN93 was 32 nM, while the concentration of the protein HIV-1 RT varied from 30 nM to 50 nM. Separation was carried out in a 25-cm capillary. Other conditions were the same as those shown in Figure 3.4.

3.3.4 Difference in FP Values and possible FRET

The FP values of all the complexes are summarized in Table 3.2.

Table 3.2 Average FP of Complexes and Unbound Aptamers

Name	1:1 Complex	1:2 Complex	Unbound Aptamers
RT12	0.127 ± 0.026	0.060 ± 0.011	0.020 ± 0.005
RT26	0.121 ± 0.028	0.039 ± 0.005	0.019 ± 0.004
RT1t49	0.125 ± 0.024	N/A	0.018 ± 0.003
ODN93	0.124 ± 0.027	0.076 ± 0.014	0.022 ± 0.006

* Data were obtained from peak FP values, corresponding to 3-5 measurements for average.

The observation of lower FP values of the 1:2 complexes than of the 1:1 complexes was initially surprising. The size of the 1:2 complex (a protein binding with two aptamers) is larger than that of the 1:1 complex (a protein binding with a single aptamer molecule). A higher FP value would usually be expected from a larger molecule. This is not the case when the FP values of the larger 1:2 complex and the smaller 1:1 complex were compared. Thus, possible reasons for the lower FP values of the 1:2 complexes were explored.

The most likely reason is depolarization by fluorescence resonance energy transfer (FRET) between the two identical fluorophores within the same 1:2 complex. When the proximity of two fluorophores is less than 100 Å (10 nm), and if one fluorophore is excited and the transition dipole moments are not parallel with each

other, resonance energy transfer can lead to the excitation of the other fluorophore prior to emission, resulting in a decrease of polarization. This can be monitored only by FP, not by fluorescence intensity.

The energy transfer depends on the distance between the fluorophores, the degree of spectral overlap of the absorption of the acceptor and the emission of the donor, and the relative orientation of the two fluorophores. The fluorophore, FAM (Figure 3.3) has good overlap in absorption and fluorescence emission spectra. When the protein HIV-1 RT binds with two aptamers that are labeled with FAM, the aptamers are recognized by their tertiary structures at the two binding sites of the protein, allowing the closeness of the two attached FAM molecules. One FAM moiety may act as a donor, and the other FAM in the same complex molecule serves as an acceptor.

FRET may occur when the two suitable fluorophores are within 100 Å (10 nm) in proximity. The shorter the distance is between the two fluorophores, the more strongly FRET takes place. Therefore, information on FRET has been suggested "a spectroscopic ruler" in studies of molecular interactions [17]. The observation of fluorescence depolarization, an indication of homo-FRET, suggests that the distance between the two fluorophores in the 1:2 complexes is less than 100 Å. This agrees with other reports that the distance of the two binding sites is approximately 60 Å [18-22].

The distance between the two fluorophores with the same molecules may be calculated from equation (1-12). However, the lack of supporting data and the

uncertainty of the parameters, such as the orientation factors, can lead to error and complication involving calculations [23-24].

Because of the relatively low concentration (nM) of the protein and the aptamers used in this study, FRET between the fluorophores on different complexes (i.e., at the inter-molecular level) is not likely to occur. The distance between two fluorophores of the adjacent protein-aptamer complexes is much longer than the intra-molecular distance when diffusion dominates. Therefore, only the intra-molecular FRET is considered here.

One advantage of FP detection combined with CE separation is the complementary information provided by both FP and CE. The FP values can be used as a powerful tool to monitor the CE separation peaks and to differentiate the complexes of different binding stoichiometries. Sometimes, in a complicated electropherogram when the separation is not effective due to such factors as impurities of samples, band-broadening, and dissociation of the complexes, the FP value can provide qualitative information to help identify the unbound and bound complex peaks. Furthermore, FP values may reveal more details on complex formation. The FP values of the complexes between a protein and two fluorescent aptamers (1:2 stoichiometry) also provide insight on possible homo-FRET within the same complex. In a homogeneous solution, homo-FRET may not be revealed, because little change of FP values would be observed from the sum of the complexes of both the 1:1 and 1:2 stoichiometries.

3.3.5 Effect of the Stability of Complexes on FP

It has been observed that the complex could dissociate during the separation by CE [25]. Because the K_d and the concentration of the protein and aptamers are at the nanomolar level, it is possible that complexes dissociate in the process of electrophoretic separation. This is probably the reason why the measured background in the electropherogram between the 1:2 complexes and the aptamers is always a little higher than the baseline. To force the equilibrium to the formation of protein-aptamer complexes, the use of higher concentrations of the protein is examined. The unbound protein will also migrate through the capillary, although it is not detected because it is not fluorescent at the detection wavelength. At a higher concentration of HIV-1 RT, less dissociation of the complexes is expected, leading to higher FP values of the complexes. This is indeed the case, as shown in Figures 3.12 and 3.13.

Figures 3.12 and 3.13 show the increase of FP values with the increase of the HIV-1 RT concentration. The concentration of aptamer RT12 was constant at 64 nM. There is a continuous, gradual increase in FP values when the HIV-1 RT protein is in excess (> 100 nM) (Figure 3.13), suggesting the possible stabilization of the complexes by the excess protein.

Changes in rotational diffusion may also contribute to the changes in FP values. The viscosity of the solution increases as the concentration of the protein increases. An increased viscosity will lead to less freedom of the fluorescent molecule, resulting in higher FP values. In addition, dissociated protein may bind with the free aptamer later

when migrating along the capillary. This may be a possible reason why the FP value of aptamer with complexes (~0.020) is always higher than that of the aptamer when HIV-1 RT is absent (0.013), because of the contribution from a small portion of the complexes.

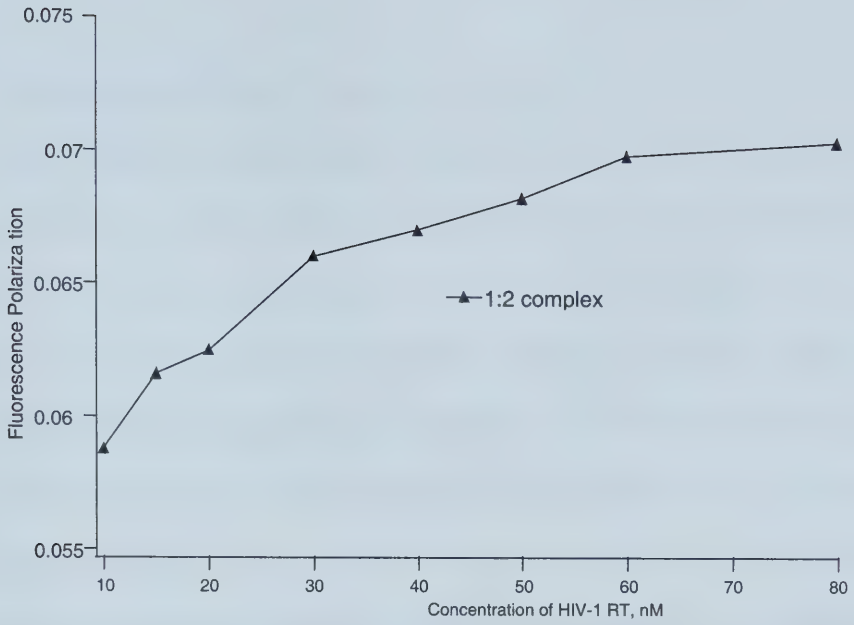

Figure 3.12 FP as a function of the HIV-1 RT concentration of the 1:2 complexes containing RT12 at 64 nM.

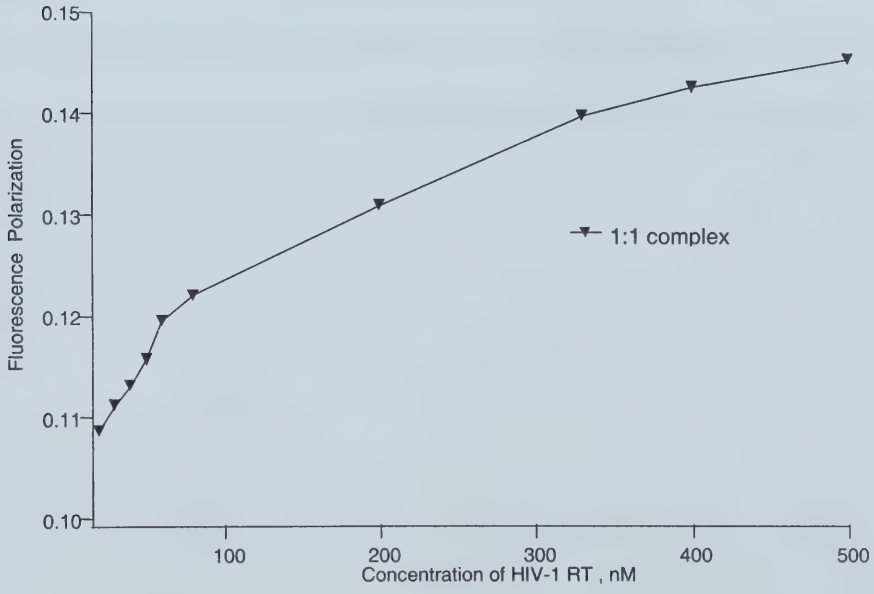

Figure 3.13 FP as a function of the HIV-1 RT concentration of the 1:1 complexes containing RT12 at 64 nM.

3.3.6 Determination of the FP value by Stop-flow

The FP values described above were obtained on-line with CE separation. The fluorescent molecules passed through the detection window quickly and were excited by the laser for only a short time (several seconds). To test if this approach is comparable with the FP measurement at "static conditions", a stop-flow method was used. When the fluorescent aptamer-protein complex migrated in the capillary to the fluorescent detection window, the electrophoretic voltage was turned off, allowing fluorescence to be detected for a desired duration (minutes). Figures 3.14 and 3.15 compare the results obtained using the on-line approach (Figure 3.14) as described in the previous sections and the stop-flow approach (Figure 3.15). In Figure 3.15, the voltage was reduced to zero between migration times from 0.8 to 1.85 min. The measured FP value is 0.127 ± 0.004 in Figure 3.15, while in Figure 3.14, the FP value of the complex peak is 0.136 ± 0.008. Both measurements are in good agreement.

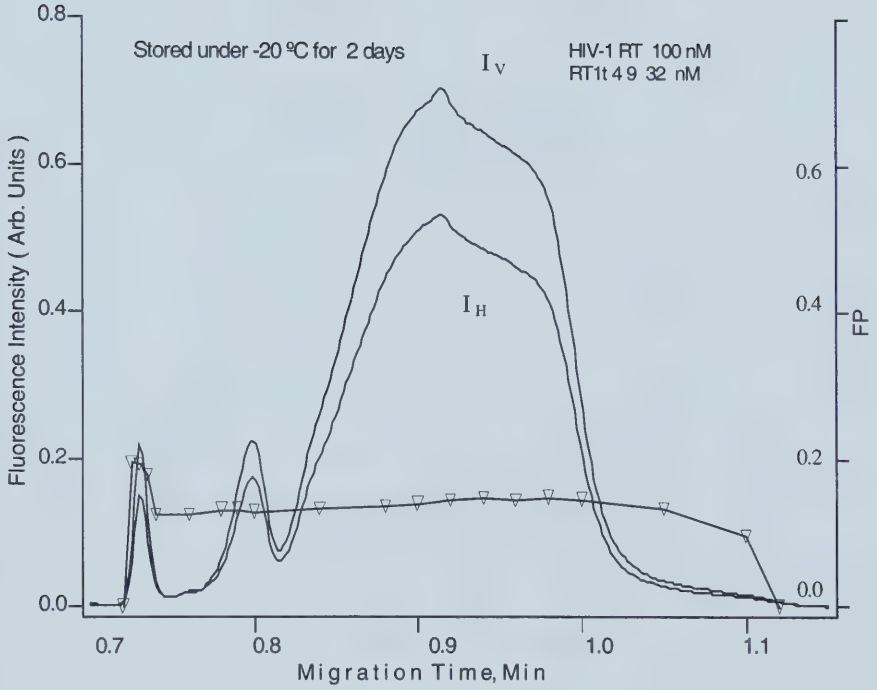

Figure 3.14 Electropherograms showing vertically- and horizontally-polarized fluorescence (the left Y-axis) and FP (the right Y-axis) of the 1:1 complex between the protein HIV-1 RT and aptamer RT1t49. I_V and I_H correspond to vertical and horizontal polarization fluorescence intensities, respectively. The concentration of RT1t49 was 32 nM, and that of HIV-1 RT was 100 nM. The sample was stored at -20 ºC for 2 days prior to analysis. The separation voltage was 20 kV.

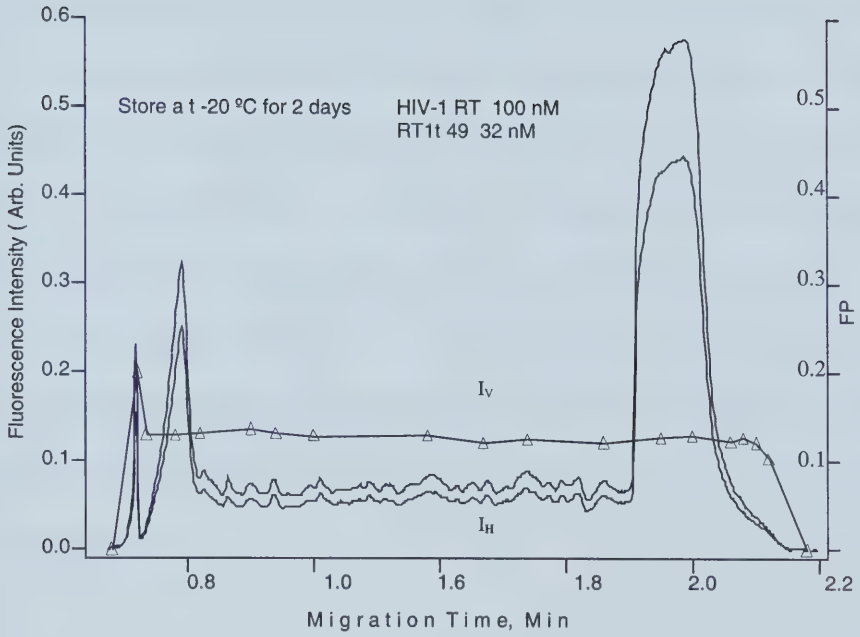

Figure 3.15 Electropherograms showing vertically- and horizontally-polarized fluorescence and FP of the 1:1 complex between the protein HIV-1 RT and aptamer RT1t49. I_V and I_H correspond to vertical and horizontal polarization fluorescence intensities, respectively. The concentration of RT1t49 was 32 nM, and that of HIV-1 RT was 100 nM. The sample was stored at -20 °C for 2 days prior to analysis. The same sample as that shown in Figure 3.14 was used. The separation voltage was 20 kV except for when it was reduced to zero between 0.8 and 1.85 min.

3.4 Conclusions

The FP of the free aptamers and the complexes has been extensively studied. The FP results support the CE results regarding the binding stoichiometries between the HIV-1 RT protein and aptamers. This protein forms both 1:1 and 1:2 complexes with aptamers RT12, RT26, and ODN93. These aptamers probably bind to both the polymerase site and RNase H site of the protein. Simultaneous on-line measurement of electrophoretic mobility and FP can be used to differentiate two stoichiometries from each other and from the free aptamers. When two aptamers bind to the protein in the 1:2 stoichiometry, the distance between the two fluorophores is probably less than 100 Å, which allows homo-FRET to occur, and leads to the depolarization of fluorescence of the 1:2 complex. When the protein binds with only one fluorescently-labeled aptamer, no depolarization of fluorescence is observed. In a multi-binding system, FP depends not only on molecular size, but also on the interactions of the fluorophores. The CE/LIFP technique can be useful for the study of other interactions, especially those involving FRET.

3.5 References

1. Lakowicz, J.R. *Principles of Fluorescence Spectroscopy* Kluwer Academic/Plenum Press, New York, **1999**
2. Rendell, D. *Fluorescence and phosphorescence Spectroscopy* Wiley, London, **1987**
3. Jameson, D.M.; Sawyer, W.H. *Methods Enzymol.* **1995**, 246, 283-300
   Fluorescence anisotropy applied to biomolecular interactions
4. Dandliker,W. B.; Kelly R. J. ;et al *Immunochemistry* **1973**, 10, 219-227
   Fluorescence polarization immunoassay. Theory and experimental method
5. Kumke, M.U.; Li, G.; McGown, L.B. *Anal. Chem.* **1995**, 67, 3945-3951.
   Hybridization of Fluorescein-Labeled DNA Oligomers by Fluorescence Anisotropy with Protein-Binding Enhancement
6. LeTilly, V.; Royer, C. A. *Biochemistry* **1993**, 32, 7753-7758.
   Fluorescence anisotropy assays implicate protein-protein interactions in regulating trp repressor DNA binding
7. Jameson, D.M.; Seifried, S.E. *Methods* **1999**, 19, 222-233
   Quantification of protein-protein interactions using fluorescence polarization
11. Wan, Q.-H.; Le, X. C. *J. Chromatogr. B* **1999**, *734*, 31-38.
    Capillary electrophoretic immunoassays for digoxin and gentamicin with laser-induced fluorescence polarization detection,
12. Wan Q.-H.; Le, X. C. *Anal. Chem.* **1999**, 71, 4183-4189.
    Fluorescence Polarization Studies of Affinity Interactions in Capillary Electrophoresis
13. Wan, Q.H.; Le, X. C. *Anal. Chem.* **2000**, 72, 5583-5589
    Studies of Protein-DNA Interactions by Capillary Electrophoresis/Laser-Induced Fluorescence Polarization
14. Le, X. C.; Wan, Q.-H.; Lam T.M. *Electrophoresis* **2002**, 23, 903-908
    Fluorescence Polarization detection for Affinity Capillary Electrophoresis
15. Lam, M. T.; Le, X. C. *Analyst* **2002**, 127, 1633-1637
    Competitive immunoassay for vancomycin using capillary electrophoresis
16. Schneider, D. J.; Feignon, J.; Hostomsky, Z.; Gold, L. *Biochemistry* **1995**, 34, 9599-9610

High-affinity ssDNA inhibitors of the reverse transcriptase of type 1 human immunodeficiency virus

17. Stryer, L.; Haugland, R. P. *PNAS USA* **1967**, 58, 719-726

Energy transfer: a spectroscopic ruler

18. Gao, H.Q.; Sarafianos, S.G.; Arnold, E.; Hughes, S.H. *J. Mol. Biol.* **1999**, 294, 1097–1113

Similarities and differences in the RNase H activities of HIV-1 RT and Moloney murine leukemia virus RT.

19. Schatz, O.; Mous, J.; Le Grice, S.F.J. *EMBO J.* **1990**, 9, 1171–1176

HIV-1 RT-associated ribonuclease H displays both endonuclease and 3'→5' exonuclease activity

20. Huang, H.; Chopra, R.; Verdine, G.L.; Harrison, S.C. *Science* **1998**, 282, 1669–1675

Structure of a covalently trapped catalytic complex of HIV-1 RT: implications for drug resistance

21. Götte, M.; Fackler, S.; et al *EMBO J.* **1995**, 14, 833–841

HIV-1 RT-associated RNase H cleaves RNA/RNA in arrested complexes: implications for the mechanism by which RNase H discriminates between RNA/RNA and RNA/DNA

22. Gopalakrishnan, V.; Peliska, J.A.; Benkovic, S.J. *PNAS USA* **1992**, 89, 10763–10767

HIV-1 RT: Spatial and temporal relationship between the polymerase and RNase H activities

23. Johansson, L. B.-Å.; Edman, P.; Westlund, P.-O. *J. Chem. Phys.* **1996**, 105, 10896-10904

Energy migration and rotational motion within bichromophoric molecules. II. A derivation of the fluorescence anisotropy

24. Tanaka, F. *J. Chem. Phys* . **1998**, 109, 1084-1092

Theory of time-resolved fluorescence under the interaction of energy transfer in a bichromophoric system: Effect of internal rotations of energy donor and acceptor

25. German, I.; Buchanan, D.D.; Kennedy, R.T. *Anal. Chem.* **1998**, 70, 4540-4545.

Aptamers as ligands in affinity probe capillary electrophoresis

Chapter 4 Denaturation and Storage Effect on Complex Formation

4.1 Introduction

4.1.1 Denaturation of protein

Denaturation is a phenomenon that involves the transformation of a well-defined, folded structure of a protein, formed under physiological conditions, to an unfolded state under non-physiological conditions [1-2]. There are many causes of protein denaturation:

- temperature changes
- non-polar solvents or H-bonding agents
- strong acids and bases
- salt concentration
- heavy metal ions such as Hg^{2+} and Pb^{2+}
- oxidants or reducing agents
- mechanical stresses such as high pressure

Denaturation may alter the secondary, tertiary, or quaternary structure of molecules, leading to loss of enzymatic activity, destruction of toxins, improvement of digestibility, loss of solubility, and change in the texture of the protein. There are several characteristics of protein denaturation:

- the conversion of a biologically functional molecule into a non-functional form
- there are many denatured states but only one native state

- proteins can regenerate to their native state but only at a slow rate
- denatured proteins have a greater tendency to aggregate

Usually denaturation is a slowly reversible process; the denatured protein folds its configuration into its native form [3-5]. However, exposing the protein to high temperature may render the process irreversible. Heat increases the kinetic energy of the protein chain and breaks the relatively weak hydrogen bonds and the electrostatic and hydrophobic interactions. The protein chain is then free to rearrange itself. Once it has cooled down enough, the protein may not be able to reorganize itself into its native structure correctly, resulting in loss of activity. Heat denaturation (98°C) was employed in this study to test the stability of the complexes between aptamers and HIV-1 RT.

4.1.2 Denaturation of DNA

DNA denaturation refers to an unwinding of the double-stranded DNA that generates two complementary single DNA strands [6-9]. This involves the breaking of hydrogen bonds between the bases in the duplex. There are three conditions that favor denaturation (also known as melting), which are: high temperature, low salt concentrations, and high pH. The most common method is to heat the DNA to a temperature above its melting point. When cooled down rapidly, the two single strands will remain the same; when renatured under stringent conditions, the two single strands will re-form the original double-stranded (ds) DNA. Any single-stranded (ss) piece of DNA can hybridize with another only if both their sequences are complementary. When one single-stranded DNA is heated and then cooled down slowly, it is possible to pair

some bases together to form a dimer; then, the secondary structure is greatly changed, and it is possible to reduce the affinity of binding to the protein. Thus, when working with heat-denatured aptamers, it is better to cool down the samples rapidly from a high temperature to 0°C to avoid dimer formation. For the ss-DNA aptamers used in this research, the secondary structures of the aptamers are important for the protein to recognize the DNA. Avoiding dimer formation is as important as the ds-DNA denaturation protocol.

4.1.3 Storage of Samples

Because protein structures are held together by non-covalent forces, they are easily destroyed by relatively mild sample storage conditions. Sample storage at room temperature will lead to denaturation of the protein, causing changes in the protein's conformation, which is necessary to bind the aptamers. Since the conformation is necessary for binding the aptamers, this results in the dissociation of the affinity complex. Usually, freezing is best for long-term storage of protein, to reduce thermal or spontaneous denaturation. DNA is relatively more stable at room temperature; however, storage of DNA samples in room temperature is not favored in this study, because of degradation of the DNA strands. Most of the samples were stored at -20°C, to maintain them with the least change possible during storage. Several samples were stored at room temperature to test the stability of the complexes formed between the aptamer RT12 and the protein HIV-1 RT.

4.2 Experimental

The home-built CE coupled with the LIFP instrument has been described previously in Chapter 2. The typical length of the capillaries was 40 cm, and the applied electric field was 500 V/cm. Unless stated otherwise, 1 × Tris-glycine was used as running buffer. The separation was carried out at ambient temperature. Other experimental procedures were the same as described in Chapter 2.

The temperature used to perform the denaturation of HIV-1 RT and RT12 was 98°C. HIV-1 RT was exposed to heat for 1 min in a heater and then cooled down gradually, allowing at least 60 min for the drop to room temperature. RT12 was heated to 98°C in a heater for 5 min, and then placed into an icebox with temperature below 4°C, immediately after being withdrawn from the heat source. All the containers of the mixture were kept closed to avoid evaporation, and were kept away from direct light to avoid photo bleaching of the dye.

All solutions were prepared in the same way as discussed in Chapter 2. All samples, when not used, were stored at -20°C in the dark.

4.3 Results and discussion

4.3.1 Effect of Denaturation

Figure 4.1 represents the effect of denaturation on HIV-1 RT and aptamer RT12. After HIV-1 RT was exposed for 1 min to 98°C and mixed with RT12, no affinity complex peak is observed in the electropherogram. The only peak is the free aptamer (the lower two electropherograms). It seems that exposure of the protein to high

temperatures results in the loss of protein binding affinity, probably because of a change of its initial conformation that is crucial for binding with aptamer RT12.

However, heating the aptamer followed by rapid cooling has little effect on its binding with the protein. After the denaturation of the aptamer (5 min at 98 °C, then rapid cooling down to 0 °C, stored 10 minutes for future use), the 1:1 complex and 1:2 complex re-form with non-denatured HIV-1 RT, depending on the molar ratio of HIV-1 RT and the aptamer. The aptamer peak disappears completely when the protein is in much excess (the top electropherogram in Figure 4.1), similar to the behavior observed in Chapter 2. The peak area and FP values of the complexes formed with denatured RT12 are identical to those of the complexes formed with non-denatured RT12. This shows an important property of the DNA aptamer. However, when the labeled aptamer is exposed to room temperature for a long period of time, it may gradually lose its ability due to the breakdown of the attached fluorophore or DNA strand. Therefore, RT12 was stored at

-20°C when not in use.

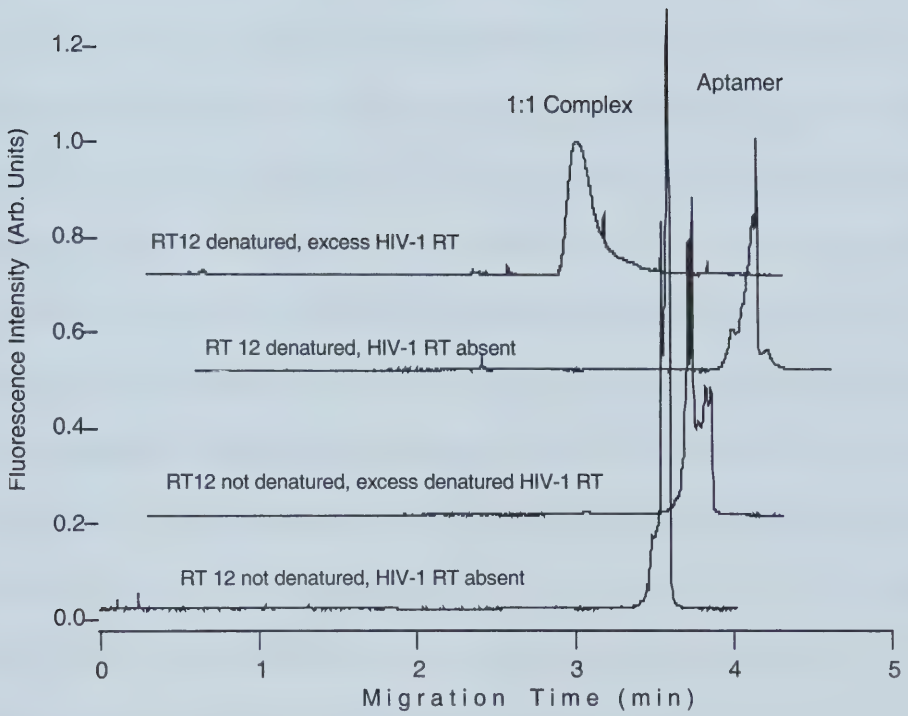

Figure 4.1 Electropherograms showing the effect of denaturation of either the protein or aptamer RT12 on the formation of the protein-aptamer complex. The concentration of aptamer RT12 was 16 nM. The same CE/LIFP conditions as shown in Figure 2.2 were used. Excess HIV-1 RT (100nM) was added to form a complex with the aptamer.

4.3.2 Effect of Sample Storage

Several samples of the mixture containing 16 nM aptamer RT12 and 100 nM HIV-1 RT were stored at -20°C and at room temperature for over 60 days to test the stability of complexes formed between the aptamer and the protein. When the mixture was stored at -20°C for 45 days, no dissociation of the complex was observed. Excess HIV-1 RT protein was used in this study. When the sample mixture was taken out from the -20°C freezer and was left at room temperature for another 11 days, the 1:1 complex peak decreased, while the 1:2 complex and the free aptamer peaks appeared. After the mixture was kept for another 14 days at room temperature, the complexes dissociated completely, and only the aptamer peak was detected in the electropherogram (Figure 4.2). These results show that HIV-1 RT was not as stable as the aptamer at room temperature over time *in vitro*, as it lost its activity to bind the aptamer after being stored at room temperature. After excess un-denatured HIV-1 RT was added to the stored mixture, the 1:1 complex still formed (1:1 stoichiometry is preferable when the protein is present in excess). The aptamer kept its ability to bind with HIV-1 RT after storage. The FP values of the complexes and the free aptamer have been measured simultaneously, and they are identical to those studied before.

Long-term storage at -20°C for over one year has been studied as well. HIV-1 RT is more likely to keep its original conformation when stored at -20°C when it is bound to the aptamer. When the unbound protein was stored for 6 months, it showed lower affinity than the samples stored with the aptamer (data not shown).

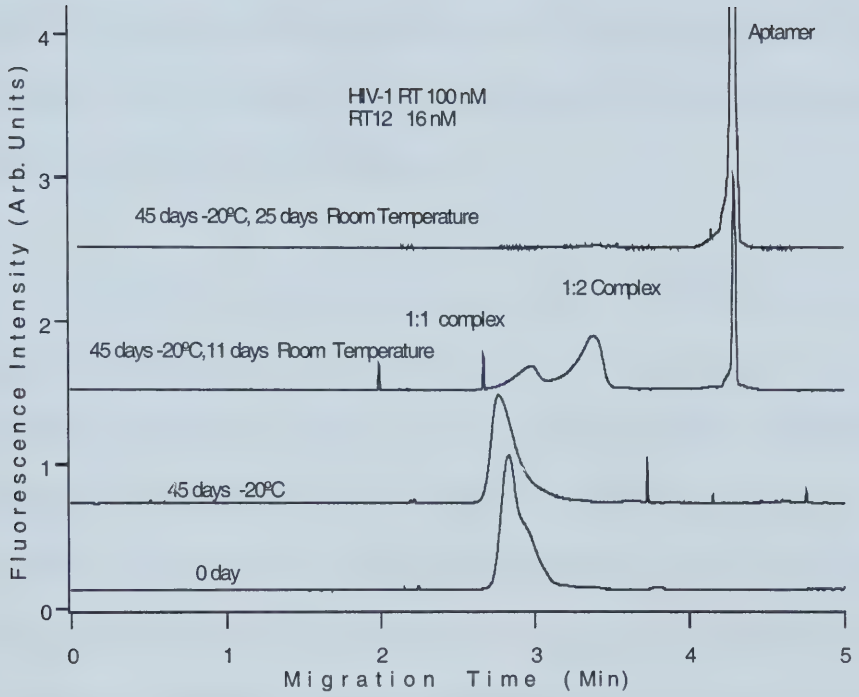

Figure 4.2 Electropherograms showing the effect of various storage conditions on the stability of the protein-aptamer complexes. The sample mixture was first stored at -20°C for 45 days, and then for another 11 and 25 days at room temperature. The concentration of aptamer RT12 was 16 nM, and that of HIV-1 RT was 100 nM. The same CE/LIFP conditions as shown in Figure 2.2 were used. Excess HIV-1 RT (100 nM) was added to form a complex with the aptamer.

4.3.3 Aggregation of Protein on Formation of X:1 Stoichiometry

Sometimes, when the stored sample has a protein-to-aptamer molar ratio greater than 3:1, small sharp peaks can be observed in CE separation after the frozen sample is re-melted. They have migration times shorter than that of the complex of 1:1 stoichiometry, as shown in Figure 4.3 (also shown in Figure 3.15 and 3.16). Usually, these small peaks are not well resolved with the 1:1 complex, and have FP values higher than those of the 1:1 complex. These peaks are likely due to complexes between aggregates of the protein and the aptamers.

HIV-1 RT has a tendency to aggregate at high concentrations [10], and this is more likely to happen in the freeze-and-thaw cycles. When the stored frozen sample melted at near 0°C, the 1:1 complex could aggregate with another unbound protein molecule, possibly to form 2:1 or 3:1 stoichiometry. Probably only a very small fraction of the HIV-1 RT protein at the nM concentration aggregated with the 1:1 complex, leading to the detection of small sharp peaks. These peaks show higher FP values than those of the 1:1 complexes, consistent with their larger size compared to the 1:1 complexes. These aggregates would be more positively-charged than the 1:1 complex, explaining their shorter migration times compared to the 1:1 complexes. However, the results are not often reproducible, probably because the aggregates are less stable than the 1:1 and 1:2 complexes between the protein and the aptamers.

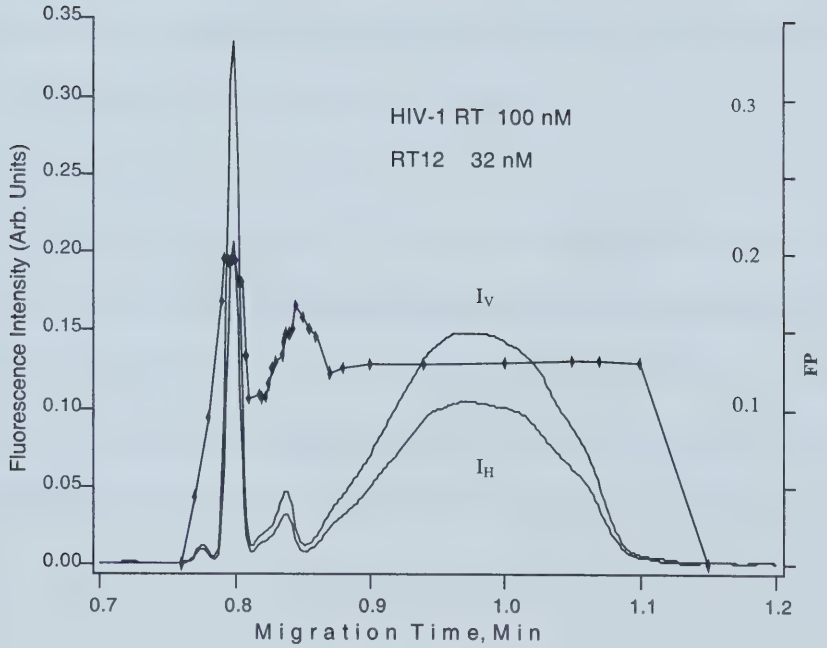

Figure 4.3 An electropherogram showing the vertically- and horizontally-polarized fluorescence and FP of protein-aptamer complexes. I_V and I_H correspond to the vertical and horizontal polarization fluorescence intensities. The concentration of RT12 was 32 nM, and that of HIV-1 RT was100 nM. The length of the capillary was 25 cm., and the electrophoretic voltage was 20 kV. Other conditions were the same as in Figure 2.2.

4.4 Conclusion

The effect of denaturation of protein HIV-1 RT and aptamer RT12 on the formation and stability of the protein-aptamer complexes has been studied. While the protein loses its binding ability when heat-denatured, heat denaturation has little effect on the binding ability of the aptamer. When stored at -20°C, the protein-aptamer complex is relative stable. At room temperature, however, the protein loses binding affinity more than the aptamer, resulting in the dissociation of the complexes. DNA aptamers may be used to study the stability of proteins.

The combined information on FP values and electrophoretic mobility (migration time) provides indications of possible protein aggregates that are associated with the aptamers. The higher FP values and shorter migration times than those of 1:1 complexes between the protein and the aptamers suggest that each aptamer is associated with more than one protein molecule in these aggregates. These aggregates are less stable than the 1:1 and 1:2 complexes between the protein and the aptamers.

4.5 Reference

1. Lapanje, S. *Physicochemical Aspects of Protein Denaturation* A Wiley-Interscience Publication, New York, 1978
2. Creufhton, T.E. (ed.) *Protein Structure: A Practical Approach* IRL Press at Oxford University Press, NY, 1997
3. Yadav, S.; Ahmad, F. *Anal. Biochem.* **2000**, 283, 207-213
   A New Method for the Determination of Stability Parameters of Proteins from Their Heat-Induced Denaturation Curves
4. Pfeil, W. *Protein Stability and Folding: A Collection of Thermodynamic Data* Springer, Berlin, **1998**
5. Arakawa T.; Hung L.; et al *Anal. Biochem.* **1993**, 208, 255-259
   Analysis of the Heat-Induced Denaturation of Proteins Using Temperature Gradient Gel Electrophoresis
6. Wartell, R. M.; Benight, A. S. *Phys. Rep.* **1985**, 126, 67-107
   Thermal denaturation of DNA molecules: A comparison of theory with experiment
7. Frank-Kamenetskii, M. D. *Physics Reports* **1997**, 288, 13-60
   Biophysics of the DNA molecule
8. Cheng, Y. –T.; Pettitt, B. M. *Prog. Biophys. Mol. Biol.* **1992**, 58, 225-257
   Stabilities of double- and triple-strand helical nucleic acids
9. Morrison, L.E.; Holder, T.C.; Stools, L .M. *Anal. Biochem.* **1989**, 183, 231-244
   Solution-phase detection of polynucleotides using interacting fluorescent labels and competitive hybridization
10. Bhikhabhai, R.; et al *J. Chromatogr.* **1992**, 604, 157-170
    Purification, characterization and crystallization of recombinant HIV-1 RT

Chapter 5 Measurement of HIV-1 RT by Using Aptamer RT12 as A Fluorescent Probe

5.1 Introduction

Many techniques have been employed to study DNA-protein binding interactions, including fluorescence spectroscopy [1], nuclear magnetic resonance (NMR) [2], mass spectrometry [3], and gel electrophoresis [4], of which the most common is the gel electrophoresis mobility shift assay (EMSA) [5-6]. CE/LIF assays have been developed to provide fast and sensitive methods to study DNA-protein binding interactions. CE/LIFP provides additional FP values of the complexes formed between DNA and proteins, which can be used to differentiate between various complexes.

Pavski and Le have developed an assay using DNA aptamer RT26 to detect HIV-1 RT at the nanomolar range; the linear region is 0-50 nM [7]. However, the assay did not differentiate between the two stoichiometric complexes formed between HIV-1 RT and aptamer RT26. Therefore, the assay is re-examined using another aptamer, RT12, and taking into account both 1:1 and 1:2 complexes.

5.2 Experimental

The home-built CE coupled with the LIFP instrument was described previously in Chapter 2. The typical length of the capillaries was 40 cm, and the applied electric field was 500 V/cm. Unless stated otherwise, 1 × Tris-glycine was

used as running buffer. The separation was carried out at ambient temperature. Other experimental procedures were the same as those described in Chapter 2.

5.3 Results and discussion

The focus of this chapter is to establish calibrations using separate measurements from the unbound aptamer and the 1:1 and 1:2 complexes between the protein and aptamer RT12. One set of calibration curves was obtained by keeping the concentration of the aptamer constant at 32 nM and increasing the concentration of the protein HIV-1 RT, as shown in Figure 5.1 and Figure 5.2. The peak area of the 1:2 complex increases to its maximum value when the concentration of the protein HIV-1 RT reaches 35 nM, then gradually decreases to its minimum at 100 nM of HIV-1 RT. The 1:1 complex appears at HIV-1 RT concentration of 20 nM, and is gradually saturated when the protein concentration exceeds 50 nM. At the same time, the peak area of the unbound aptamer RT12 decreases with the increase of the 1:1 complex. The increase of total peak area of the two complexes is mirrored with the decrease of the peak areas from the unbound aptamer (Figure 5.2).

An expanded region (0-35 nM) of the calibration curve is shown in Figure 5.3 when the total peak area of the two complexes was used as response. The peak area of the complexes is linear from 0-35 nM of HIV-1 RT concentration, with an r^2 value of 0.985. Alternatively, when the peak area of the unbound aptamer RT12 was used for calibration, a calibration curve is shown in Figure 5.4 for the same linear region, with an r^2 value of 0.980. Similar results have been obtained by keeping the concentration of

RT12 constant at 64 nM, and varying the concentration of HIV-1 RT. These results suggest that the fluorescently-labeled aptamer RT12 can be used as a probe to detect HIV-1 RT protein at nM levels. When two protein-aptamer complexes are measured, the sum of their measurements can be used for calibration. The measurement of the unbound aptamer can also be used for calibration. CE/LIFP offers a useful method for the determination of HIV-1 RT protein concentration.

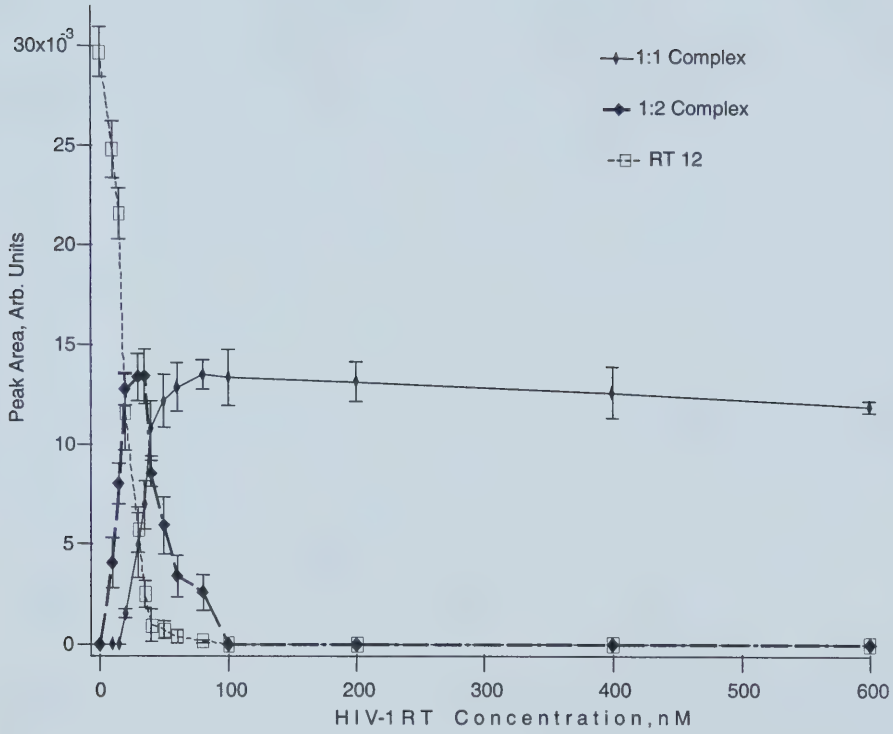

Figure 5.1 Calibration curves constructed using the samples containing 32 nM aptamer RT12. The peak areas of the 1:1 and 1:2 complexes and the unbound aptamer RT12 were measured separately. All error bars represent the standard deviation from 3 to 5 runs. The same CE/LIFP conditions as shown in Figure 2.2 were used.

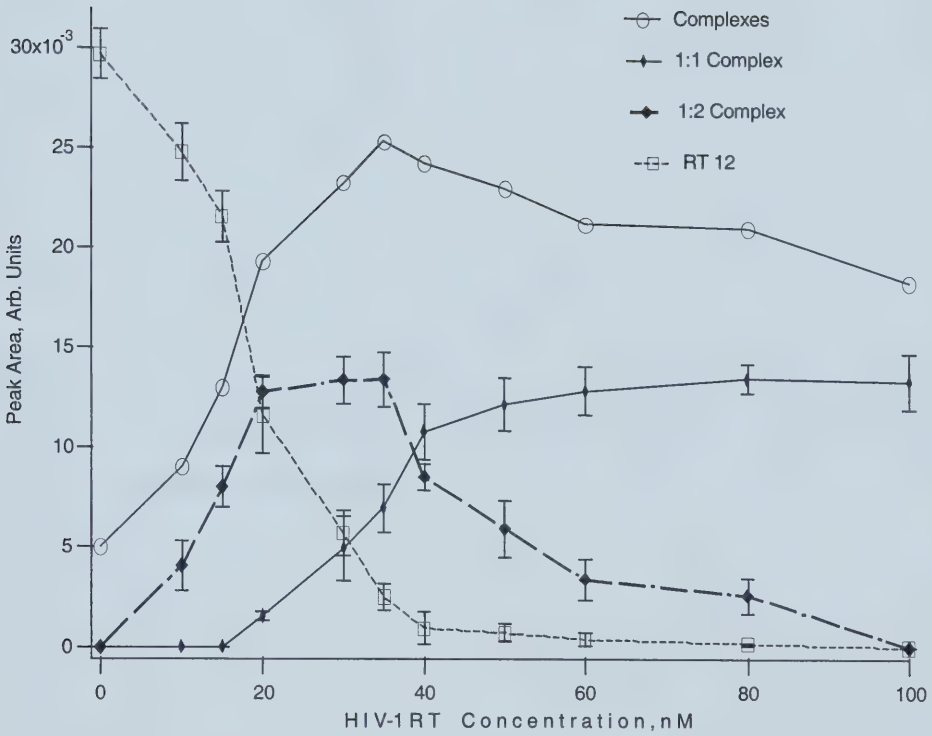

Figure 5.2 An expanded region of calibration curves shown in Figure 5.1. The upper solid line represents a calibration between the sum of the peak areas of the two complexes and the concentration of the HIV-1 RT protein. This curve is Y-axis offset for clarity. The same conditions as shown in Figure 5.1 were used.

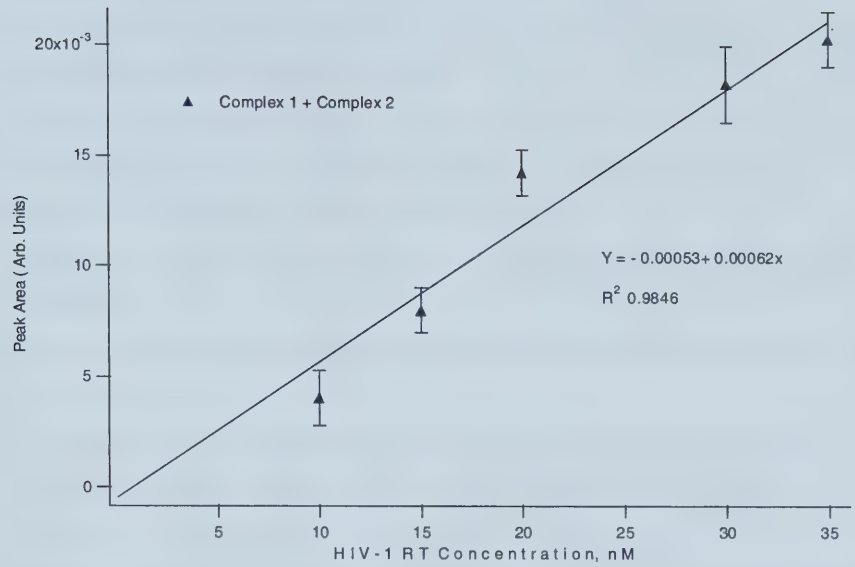

Figure 5.3 Linear region of calibration between the peak area of the two complexes and the concentration of HIV-1 RT (0-35 nM). The same conditions as in Figure 5.1 were used.

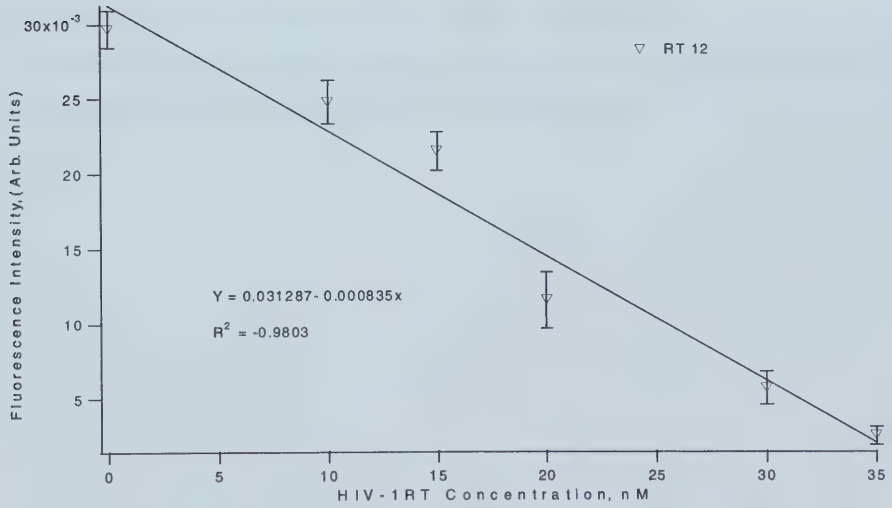

Figure 5.4 Linear region of calibration between the peak area of the unbound RT12 and the concentration of HIV-1 RT (0-35 nM). The same conditions as in Figure 5.1 were used.

5.4 References

1. Kwon, K.; Stivers, J.T. *J. Biol. Chem.* **2002**, 277, 345-352
   Fluorescence spectroscopy studies of vaccinia type IB DNA topoisomerase. Closing of the enzyme clamp is faster than DNA cleavage
2. Dangi, B.; Pelupessey, P.; et al *J. Mol. Biol.* **2001**, 314, 113-127
   Structure and Dynamics of MarA-DNA Complexes: An NMR Investigation
3. Veenstra, T.D. *Biophys. Chem.* **1999**, 79, 63-79
   Electrospray ionization mass spectrometry in the study of biomolecular non-covalent interactions
4. Levit, M.N.; Abramczyk, B.M.; Stock, J.B.; Postel, E.H. *J. Biol. Chem.* **2002**, 277, 5163-5167
   Interactions between Escherichia coli nucleoside-diphosphate kinase and DNA
5. Fried, M.; Crothers, D.M. *Nucl. Acids Res.* **1981**, 9, 6505-6525
   A Gel Electrophoresis Method for Quantifying the Binding of Proteins to Specific DNA Regions: Application to Components of the Escherichia Coli Lactose Operon Regulatory System
6. Grove, A.; Lim L. *J. Mol. Biol.* **2001**, 311, 491-502
   High-affinity DNA binding of HU protein from the hyperthermophile Thermotoga maritime
7. Pavski, V.; Le, X. C. *Anal. Chem.* **2001**, 73, 6070-6076.
   Detection of Human Immunodeficiency Virus Type 1 Reverse Transcriptase Using Aptamers as Probes in Affinity Capillary Electrophoresis

Chapter 6 Conclusion and Future Work

CE/ LIFP combines the advantages of CE — small sample size, minimal sample preparation, high resolution, as well as speed of analysis — with the advantage of FP, which provides information on the size of all separated components. The separation of the complexes formed between DNA aptamers and HIV-1 RT protein and the measurement of the FP values of all components lead to the determination of the 1:1 and 1:2 stoichiometry of the complexes. All aptamers form the 1:1 stoichiometry with the protein. The fluorescence depolarization of the 1:2 complexes between the protein and the aptamers RT12, RT26, and ODN93 was probably caused by homo-fluorescence resonance energy transfer, indicating that the distance between two fluorophores in the same protein-aptamer complex is below 100Å. The ACE method can be applied to directly and selectively detect HIV-1 RT quantitatively. ACE combined with LIFP is a powerful tool to study multi-binding systems of DNA and proteins.

Future research can focus on different inhibitors that are competitive with aptamers, such as other NRTIs (nucleoside RT inhibitors) and NNRTIs (non-nucleoside RT inhibitors), or on aptamers that are competitive with each other. The purity of HIV-1 RT needs to be checked by gel electrophoresis. Aptamers that form 1:2 stoichiometries may be applied to two-site binding assays for diagnostic use. Aptamers may have been modified differently to test their affinity with target molecules, or to test the affinity of the modified protein by CE/LIF. Another

direction is to look for auxiliary proteins that stabilize the complexes formed to achieve higher sensitivity in this assay. Furthermore, a new multi-binding system can be designed to monitor the change of distance between the binding sites by the measurement of FP to monitor homo-FRET, making the distance under or over the R_0 of the dye attached to the probes.

University of Alberta Library
0 1620 1829 9766
B45836